3-22-2019

Coupled Atmospheric Surface Observations with Surface Aerosol Particle Counts for Daytime Sky Radiance Quantification

Scott S. Wolfmeyer

Coupled Atmospheric Surface Observations with Surface Aerosol Particle Counts for Daytime Sky Radiance Quantification

THESIS

Scott S. Wolfmeyer, 1st Lt, USAF

AFIT-ENP-MS-19-M-095

DEPARTMENT OF THE AIR FORCE
AIR UNIVERSITY

AIR FORCE INSTITUTE OF TECHNOLOGY

Wright-Patterson Air Force Base, Ohio

DISTRIBUTION STATEMENT A
APPROVED FOR PUBLIC RELEASE; DISTRIBUTION UNLIMITED.

AFIT-ENP-MS-19-M-095

COUPLED ATMOSPHERIC SURFACE OBSERVATIONS WITH SURFACE AEROSOL PARTICLE COUNTS FOR DAYTIME SKY RADIANCE QUANTIFICATION

THESIS

Presented to the Faculty
Department of Engineering Physics
Graduate School of Engineering and Management
Air Force Institute of Technology
Air University
Air Education and Training Command
in Partial Fulfillment of the Requirements for the
Degree of Master of Science in Applied Physics

Scott S. Wolfmeyer, B.A.
1st Lt, USAF

21 Mar 2019

DISTRIBUTION STATEMENT A
APPROVED FOR PUBLIC RELEASE; DISTRIBUTION UNLIMITED.

AFIT-ENP-MS-19-M-095

COUPLED ATMOSPHERIC SURFACE OBSERVATIONS WITH SURFACE AEROSOL PARTICLE COUNTS FOR DAYTIME SKY RADIANCE QUANTIFICATION

THESIS

Scott S. Wolfmeyer, B.A.
1st Lt, USAF

Committee Membership:

Dr. S. T. Fiorino, Ph.D.
Chair

Maj. M. R. Ferdinandus, Ph.D.
Member

Dr. K. J. Keefer, Ph.D.
Member

Abstract

Many applications of multi- and hyperspectral imaging, detection, and tracking from ground to space like space situational awareness (SSA) are often limited to nighttime hours due to solar background noise. For daytime ground-based multi- and hyperspectral imaging it is extremely important to be able to quantify the background noise of the sky in the ultraviolet to near infrared range of the electromagnetic spectrum. Daytime sky radiance can be characterized in any direction at any time using the Laser Environmental Effects Definition and Reference (LEEDR) atmospheric characterization and radiative transfer code provided there is enough real-time observed information. Real- or near real-time information needed for sky radiance calculations includes temperature, pressure, humidity, and aerosol concentration that is present throughout the atmospheric path.

This research investigates the important questions of how much real-time information is needed, how difficult is it to obtain, and whether or not some or all the inputs need to be measured or diagnosed/predicted, e.g. obtained from numerical weather prediction (NWP). LEEDR can utilize the real or near real-time information from radiosondes, satellites, and surface weather stations. In addition, LEEDR can also ingest NWP data and some combination of observations plus climatology as well as utilize aerosol optical depths from sunphotometers. The hypothesis this research seeks to evaluate is the easiest and nearly most accurate method for LEEDR to diagnose sky radiance for any viewing angle is to combine surface meteorological (MET) observations with surface aerosol particle concentrations.

In order to evaluate what is optimal in terms of ease of obtaining the necessary data as well as the accuracy and speed of the analysis, sky radiance measurements

were made using a telescope and spectrometer for a select number of non-winter days that were sunny and clear and offered varying atmospheric conditions. LEEDR sky radiances were calculated for the given days, times, and telescope look angles for each of the real-time observed surface observations (pressure, temperature, humidity, aerosol concentrations) and NWP data as well as all combinations of those observations and NWP data. Comparisons were made between the sky radiance measurements and the LEEDR radiance outputs to determine what combinations of real-time observed information produced the most accurate models.

Acknowledgements

First, I would like to thank my thesis advisor, Dr. Steve Fiorino, for providing his expert guidance, assistance, and seemingly unlimited energy that helped make this research successful as well as enjoyable. I would also like to recognize Maj. Grant Thomas whose dissertation research provided the necessity for this thesis as well as his help and knowledge to make this research a success.

Secondly, I need to thank Dr. Kevin Keefer for his assistance in operating the atmospheric and environmental instrumentation as well as Jaclyn Schmidt and Brannon Elmore for their expertise in the operation of the key simulation tool used in this research. I would also like to thank the other members of my committee and the faculty for their valuable contributions, expertise, and feedback that contributed throughout the thesis process.

Next, I want to thank my friends and family for all the support that they have and still do provide towards my military career and academic endeavors. Finally, I would be remiss if I didn't recognize and thank my fellow classmates for all of the help and collaboration they provided these past 18 months. All of you helped contribute, in one way or another, not only to my research success but also to my successful understanding of the necessary academic knowledge. I wish you all nothing but happiness and success in your military careers moving forward.

Scott S. Wolfmeyer

Table of Contents

Page

List of Figures

List of Tables

List of Acronyms

AzEl azimuth and elevation

BL boundary layer

CFCs chlorofluorocarbons

CO carbon monoxide

CO_2 carbon dioxide

CPC Condensation Particle Counter

EM Electromagnetic

ExPERT Extreme and Percentile Environmental Reference Tables

GADS Global Aerosol Data Set

GEO geostationary

GFS Global Forecast System

GHz gigahertz

H_2O water vapor

HITRAN HIgh-resolution TRANsmission

IR infrared

LEEDR Laser Environmental Effects Definition and Reference

LWIR longwave infrared

mb millibar

MET meteorological

MHz megahertz

MODTRAN MODerate Resolution Atmospheric TRANsmission

MWIR mid wave infrared

N_2O nitrous oxide

NCEI National Centers for Environmental Information

NCEP National Centers for Environmental Prediction

NH_4 methane

NIR near-infrared

NOAA National Oceanic and Atmospheric Administration

NOMADS NOAA Operational Model Archive and Distribution System

NWP numerical weather prediction

O_2 oxygen

O_3 ozone

OPAC Optical Properties of Aerosols and Clouds

RADAR Radio Detection and Ranging

RH relative humidity

SSA space situational awareness

SWIR shortwave infrared

TOD Time of Day

USAF United States Air Force

UTC Coordinated Universal Time

UV ultraviolet

WPAFB Wright-Patterson Air Force Base

I. Introduction

1.1 Background

A fundamental component required for successfully operating in space is space situational awareness (SSA). A key element that is integral for effective SSA is the ability to identify and track space assets as they orbit the Earth. The ability to have persistent accountability of space assets provides the capability to avoid collisions, perform maneuvers, as well as other necessary functions. In order to be able to track space assets at every point in orbit, there is a network of optical and radar detectors around the world providing worldwide coverage. A big issue for the persistent accountability of space assets is the capability to track those assets during the daylight hours.

During the night, detectors have few issues detecting objects orbiting the Earth because the atmospheric scattering of moon and stellar light does not produce enough radiance to mask the signal from the satellite. During the day, the Sun produces an overwhelming amount of energy in the visible and near-infrared (NIR) part of the electromagnetic spectrum which greatly inhibits optical detectors from sensing reflected light from an orbiting satellite. Current research into daytime space asset tracking confirms that the Sun produces the most energy or radiance in the visible spectrum [26]. The research also shows the Sun's energy diminishes as wavelengths get longer into the NIR and shortwave infrared (SWIR) spectrum [26]. The diminished solar energy at longer wavelengths is the reason radar detectors are so successful. The problem with radar detectors is there are a limited amount of them available to be used which causes gaps in the worldwide coverage. In an effort to close these gaps, it could be beneficial to utilize other detectors that sense energy at wavelengths such as in the infrared (IR) spectrum.

In order to determine if NIR and SWIR detectors would be useful, it would be advantageous to be able to characterize sky radiance from the visible to SWIR (0.4μm - 2μm). In order to characterize sky radiance, it is necessary to understand and investigate how light propagates through the atmosphere. The daytime tracking research conducted by Thomas et al.[26] also discovered that the amount of sky radiance detected was not the same throughout the day. The differences are explained by the radiative processes of absorption, emission, and scattering that affect the path of light as it propagates through the atmosphere. The radiative processes depend on a number of weather and atmospheric conditions such as temperature, pressure, humidity, aerosol content and others.

Successfully characterizing sky radiance requires solving the complex radiative transfer equation that is necessary to explain how absorption, emission, and scattering are affecting light at any given time during the day. Currently, the equation is calculated and modeled using radiative transfer codes such as Laser Environmental Effects Definition and Reference (LEEDR)[14] and MODerate Resolution Atmospheric TRANsmission (MODTRAN)[3]. The radiative transfer codes can take the necessary weather and atmospheric inputs for any given day and time and calculate the sky radiance at any wavelength. The sky radiances produced by LEEDR could be used to help distinguish actual sky radiance measurements from the signal of an orbiting space object.

1.2 Problem Statement

The issue with using a radiative transfer code such as LEEDR to obtain a characterization of sky radiance becomes ascertaining how much atmospheric information is necessary to get an accurate representation of the sky radiance. LEEDR can infer the necessary atmospheric and weather information, i.e. pressure, temperature, humidity, and particle concentrations, for the day and time in question but the resulting sky radiances may not be as accurate as they could be. If real-time observed surface and atmospheric data is provided, LEEDR can produce a more accurate characterization of the sky radiance on any given day and time. However, it would not be practical to obtain and use every piece of atmospheric data every time a characterization of sky radiance is needed. The atmospheric and weather data is not always recorded for every specific location, for specific times down to the minute, and necessary equipment is not always available. The best idea would be to determine how much information is actually necessary in order to obtain an accurate sky radiance characterization any time such information is needed.

The purpose of this thesis is to examine and determine the threshold of information that is necessary in order to produce an accurate sky radiance characterization. This thesis intends to discover what is best as far as ease of obtaining information, speed of the analysis, and most importantly the accuracy of the resulting output. In order to get expedient and more accurate sky radiance results from LEEDR, it is hypothesized the best approach is coupling surface meteorological (MET) observations of pressure, air temperature, and dew point with surface aerosol particle concentrations. This research also investigates whether applying numerical weather prediction (NWP) increases the ease and accuracy of obtaining LEEDR sky radiance characterizations.

1.3 Research Objectives

The research requires a comparison of actual sky radiance measurements with LEEDR sky radiance characterizations calculated while using observed atmospheric and weather data for the days and times in question as well as NWP data. The comparisons are used in order to achieve the following objectives of the research:

- Determine how accurate LEEDR is in generating radiance characterizations while relying only on observed surface MET conditions with climatological aerosol information from the Global Aerosol Data Set (GADS)

- Determine how accurate LEEDR is in generating radiance characterizationss while relying only on NWP data alone and observed surface aerosol information alone

- Investigate if coupling surface MET conditions, climatological aerosol information, observed aerosol information, and NWP data improves the accuracy of LEEDR radiance characterizations

1.4 Research Plan

The plan for this research is to compare real-time spectral sky radiance measurements with LEEDR simulated radiance characterizations that utilize surface MET observations, climatological or observed aerosol information, and/or NWP data. The plan is designed to determine what atmospheric and weather information allows LEEDR to successfully duplicate or nearly duplicate measured sky radiances. In order to do this, multiple spectral radiance measurements are collected on a few days at different times, separated by an hour or more. The days chosen are sunny summer days that are clear or nearly clear of clouds in order to ensure the desired aerosol-only scatter effects. The radiance measurements are found for six specific sky positions with azimuth and elevation angles corresponding to positions of the geostationary (GEO) orbital belt. By selecting several specific times and sky positions during those days, it is possible to determine how well LEEDR is able to characterize sky radiance.

When LEEDR radiance characterizations are generated, the baseline assumption is the combination of surface MET observations and observed aerosol information is enough to duplicate the measured values of sky radiances. However, it is necessary to determine if NWP can also provide information that would generate accurate radiance characterizations in LEEDR. In order to determine the accuracy of both, radiance characterizations are created with LEEDR for all real-time MET observations, aerosol information, and NWP. LEEDR radiance characterizations are generated for each individual MET observation, observed aerosol information, and NWP data alone as well as all combinations of this information. The LEEDR characterizations are then compared to the measurements found to determine which combination of inputs is the most accurate match.

1.5 Preview

The organization of this thesis document consists of an introduction, a literature review, methodology, results and analysis, and conclusion with future work. Subsequent to this introductory chapter, chapter II is intended to provide the reader background about the theory behind spectral radiance, radiative processes, and radiative transfer codes. Chapter III details the various instruments, codes, and tools used, as well as the method followed, to address the research objectives. Chapter IV conveys the results of the comparative analysis of the data and what the results mean. Chapter V draws conclusions from the analysis as well as what work should follow the conclusion of this research.

II. Literature Review

2.1 Overview

The following chapter is intended to provide necessary background knowledge and theory required to investigate and characterize spectral sky radiance. Initially, the chapter will discuss the specifics of the Electromagnetic spectrum as well as the radiometry involved to get spectral radiance. After that, the radiative transfer equation will be covered including the radiative processes that are accounted for by this equation as well as how those processes affect the way light propagates. Finally, the radiative transfer and atmospheric characterization code known as LEEDR will be described along with key processes it uses.

2.2 The Nature of Light

2.2.1 The Electromagnetic Spectrum.

Light is generally characterized into quantifiable parameters such as wavelength, frequency, and energy which makes up the Electromagnetic (EM) spectrum. The EM spectrum is further differentiated into spectral bands that can be utilized in many different ways. There are five spectral bands typically used for electro-optics and radio frequency research and applications that can be seen in Figure 1. These bands span from about 0.1μm to 100m and are designated as ultraviolet (UV) (0.1μm-0.4μm), visible (0.4μm-0.7μm), IR (0.7μm-1mm), and microwave/radio (1mm-100m and more). The five bands are further differentiated as well due to the various effects they all have in the atmosphere as well as how they are used in detection [9].

The first significant band is the UV which is broken up into four sub-bands known as the far UV, UV-C, UV-B, and UV-A. The radiation involved in the UV band is solely supplied by the sun but the amount of this radiation that reaches the

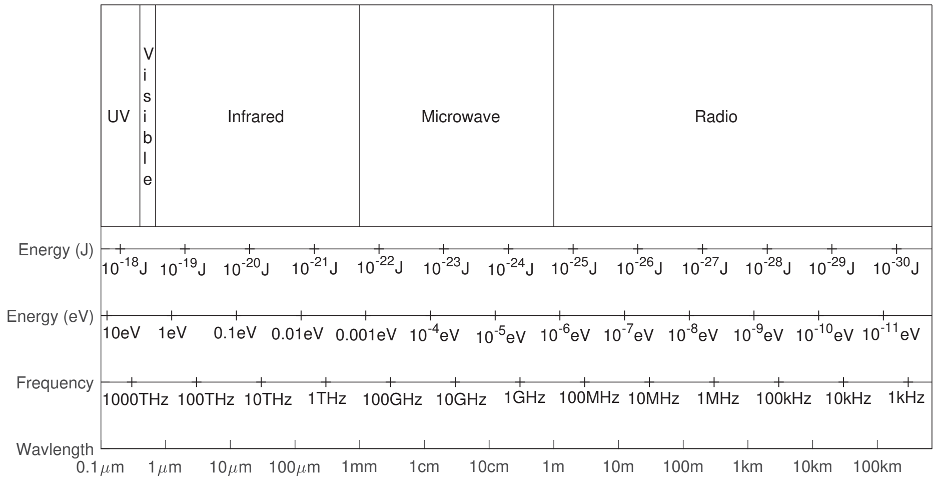

Figure 1. The Electromagnetic Spectrum showing where each region lies as well as the wavelengths, frequencies, and energies that correspond to those regions [16].

Earth's surface is very minimal [25]. Virtually all of the far UV, UV-C, and UV-B radiation gets absorbed in the top half of the atmosphere by either oxygen (O_2) or ozone (O_3) [25]. The UV-A is the only part of the UV region that actually reaches the Earth's surface and is mostly invisible to the human eye even though it is closest to the visible part of the spectrum.

The visible band of the EM spectrum spans from 0.4μm to 0.7μm and corresponds to visible light that the human eye can see [9]. The visible region also corresponds to the maximum emission of radiation by the sun and close to half of the total power of the sun falls into this band [25]. The wavelengths in and around the visible part of the spectrum are the ones that correspond to all of the colors that make up light [9]. Even though the UV is mostly invisible to the eye, the wavelengths closest to the visible spectrum correspond to the color purple. The wavelengths that are around 0.4μm are where blue starts and the colors progress to green, yellow, orange, and ends with red around 0.7μm where the IR band begins [9].

The IR band, just like the UV, is mostly invisible to the human eye except for close to the visible band where red can still be seen at some wavelengths past

$0.7\mu m$. The IR region is a very broad band of wavelengths that has numerous areas of absorption due to atmospheric constituents that include water vapor (H_2O), carbon dioxide (CO_2), methane (NH_4), and chlorofluorocarbons (CFCs) [25]. The IR region can be divided in a number of ways but the main categories to consider are the NIR ($0.7\mu m$-$4\mu m$), thermal IR ($4\mu m$-$50\mu m$), and far-IR ($50\mu m$-1mm) [25]. In some situations, there are three alternate divisions in the IR region which includes SWIR ($1\mu m$-$3\mu m$), mid wave infrared (MWIR) ($3\mu m$-$5\mu m$), and longwave infrared (LWIR) ($5\mu m$-$15\mu m$) [9].

The last of the major spectral bands are the radio and microwave bands which refer to frequency as well as wavelength to indicate the different variations in the spectrum. The microwave band spans wavelengths of 1mm to 1m or frequencies of 300 gigahertz (GHz) to 3 GHz while the radio band spans wavelengths of 1m to 100m or frequencies of 3 GHz to 3 megahertz (MHz) and lower [25]. These bands typically utilize Radio Detection and Ranging (RADAR) and are differentiated into sub-bands known as Ka, K, Ku, X, C, S, L, and P [9]. The microwave and radio bands are typically used for monitoring severe weather, connective cloud systems, wind profiles, and lightning detection [9].

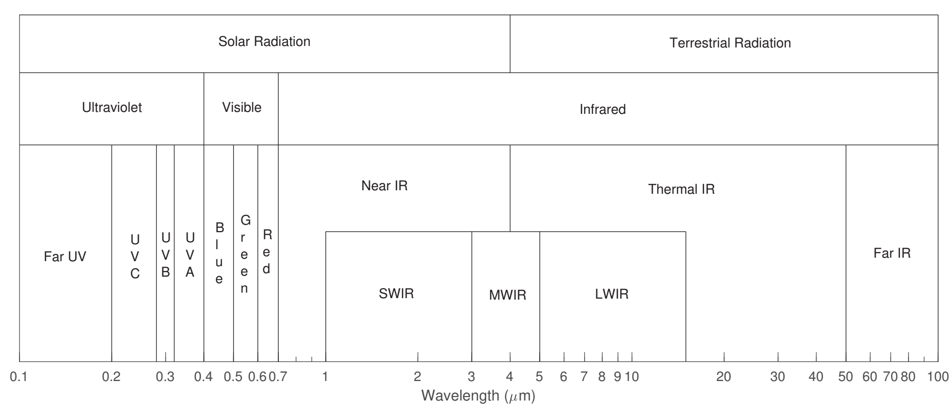

Figure 2. An illustration of the divisions in the Electromagnetic spectrum and which regions correspond to solar radiation and terrestrial radiation

Relative to the EM spectrum and this research, differentiating solar spectral energy as compared to that associated with the blackbody energy radiated by the Earth is important. As seen in Figure 2, the energy radiated by the sun, referred to as solar or shortwave radiation, is primarily in the UV and SWIR bands and mostly accounted for in the wavelength span from 0.1μm to 3μm. Figure 2 also shows Earth's radiated energy, referred to as terrestrial or longwave radiation, is accounted for in the range of 3μm to 100μm [25]. A small percentage of solar radiation is accounted for by the UV band while the visible and NIR bands equally account for the rest. Terrestrial radiation is covered by the thermal IR and the far-IR bands while microwave and radio bands do not play role in either solar or terrestrial radiation detection [25].

2.2.2 Spectral Radiance.

The discussion of solar and terrestrial radiation also leads us to the discussion of what the spectral radiance is and how to find it. A discussion about spectral radiance involves the theory of Blackbody radiation and the interactions of reflection, absorption, transmission, and emission. A Blackbody is an object that perfectly absorbs thermal radiation or, in other words, it absorbs all of the radiation that is incident upon it [4]. The concept of perfect absorption leads to the relationship called Kirchhoff's Law that says a good absorber of radiation is a good emitter of radiation. In other words, Kirchhoff's Law tells us that the absorption of a medium is the same as the emittance of that same medium [4].

The mathematical representation of the emitted radiation of a Blackbody, shown in Equation 1 where h is *Planck's Constant*, c is *the speed of light*, and k_B is *Boltzman's Constant*, was found by Max Planck as a function of wavelength and temperature [9].

$$B(\lambda, T) = \frac{2\pi hc^2}{\lambda^5} \frac{1}{exp[\frac{hc}{\lambda k_B T}] - 1} \tag{1}$$

The definition of Planck's function is given to be the total intensity of emitted radiation contributed by the interval of the wavelength. Essentially, Planck's equation defines the intensity, or power per solid angle, per unit area emitted per wavelength which in units is $W/m^2 sr\mu m$ [4]. A solid angle, shown in Equation 2 and pictured in Figure 3, conveys the viewing angle at which some surface area is being looked at on a hemisphere of some radius [4].

$$\Omega = \frac{A}{R^2} \tag{2}$$

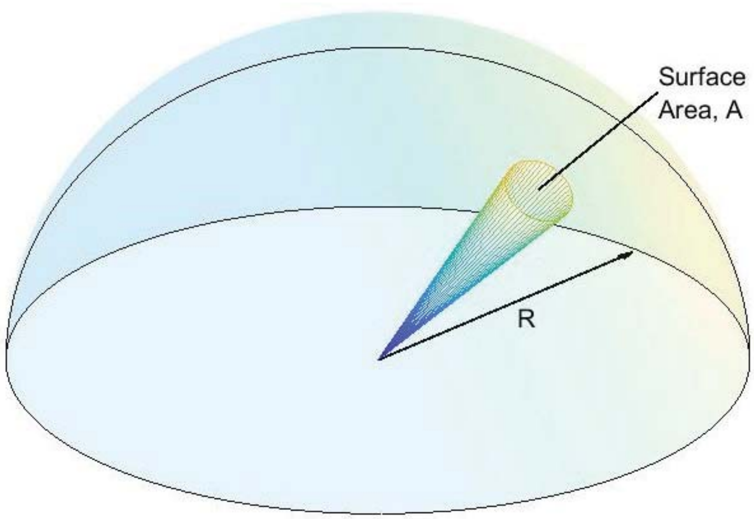

Figure 3. The solid angle illustrates the viewing angle of some area on a hemisphere.

Figure 4 shows a plot of Planck's function over all wavelengths up through the far-IR while varying the temperature from around room temperature (300K) up to the temperature of a star or the Sun (6000K) [9]. Figure 4 also shows Wien's Displacement Law which says the peak wavelength changes in a linear fashion as the temperature changes. Wien derived the mathematical function for the Displacement Law, shown in Equation 3, where the peak wavelength, λ_{max}, is found by dividing an

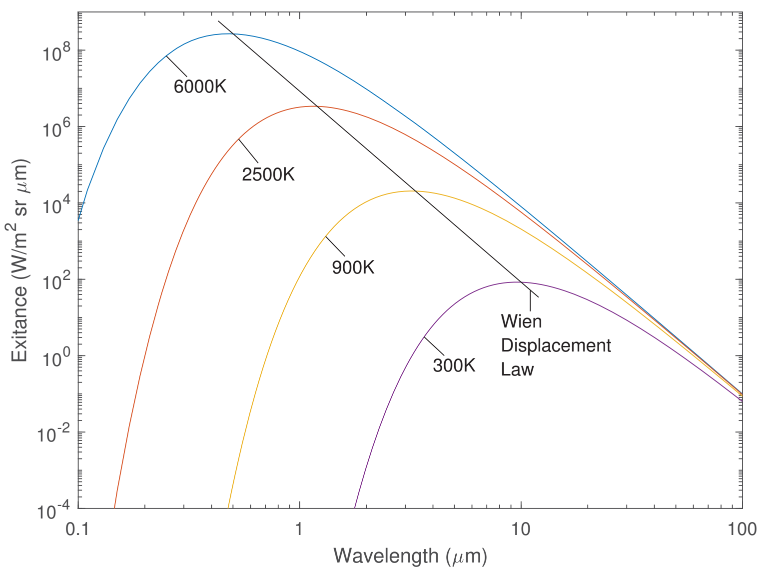

Figure 4. Planck Blackbody curves for temperatures at 300K, 900K, 2500K, and 6000K with Wien's Displacement Law shown as well.

experimental constant by the temperature [9].

$$\lambda_{max} = \frac{constant}{T} \tag{3}$$

The constant in Equation 3 was experimentally found to be about 2897.8μmK but it is also often approximated to be 3000μmK [9]. Applying Wien's Law to the temperatures above for room temperature (300K) and the Sun (6000K) produces peak wavelengths of $\lambda_{max} = 10\mu m$ and $\lambda_{max} = 0.5\mu m$ respectively [9].

The next thing to consider is how the radiometry works to get a sky radiance from the Blackbody radiation emitted by the Sun. The radiation emitted by a Blackbody source is the same thing as the exitance, M, emitted by a source of radiation and the irradiance, E, onto the surface of some target [4]. The exitance describes the amount of power of a source of radiation that is leaving it with respect to its area. The irradiance turns out to be the same as the exitance except that it is the same power per area that is received by a different surface [4]. The power that exits a

Blackbody source is the same amount of power that is received when it reaches the surface of another object.

Another important idea to remember is how the radiance relates to the exitance of whatever source it originated from. Planck's equation for Blackbody radiation includes a dependence on the solid angle but most radiation sources like the Sun are considered to be Lambertian sources. A Lambertian source is defined as a radiation source whose radiance is completely independent of the solid angle and that equal amounts of spectral radiance is found in all directions. A Lambertian source also means the exitance, shown in Equation 4, relates to the radiance by a factor of π [4].

$$M = E = \pi L \tag{4}$$

Considering the Sun as a Lambertian source and using the Blackbody equation provides a solar spectral radiance, shown in Equation 5, for all wavelengths being considered with respect to the temperature of the Blackbody source.

$$L = \frac{M}{\pi} = \frac{2hc^2}{\lambda^5} \frac{1}{exp[\frac{hc}{\lambda k_B T}] - 1} \tag{5}$$

The final concept to be considered specifically when dealing with a spherical Lambertian source is the role that distance plays in how exitance becomes the radiance. When examining a situation like the Earth and the Sun in Figure 5, the relation between the radiance and the irradiance seen in Equation 4 remains the same.

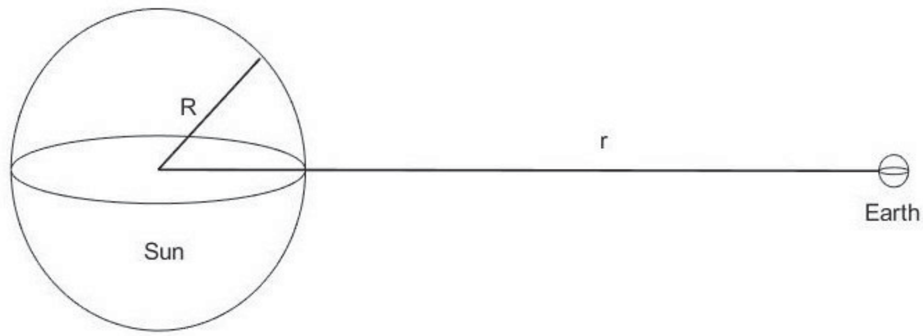

Figure 5. The exitance of the Sun becomes the irradiance upon the Earth depending on the ratio of the radius of the Sun to the distance from the center of the Sun to the Earth

However, at some distance from the center of the source, the exitance must uniformly irradiate the surface of the target. The result of this uniform irradiance of the target, shown in Equation 6, shows that the irradiance obeys an inverse-square law for any distance that the exitance has to travel [4].

$$E = \frac{R^2}{r^2}\pi L \tag{6}$$

2.3 Radiative Processes and Calculations

2.3.1 Radiative Transfer Equation.

So far, the discussion has been how the Blackbody radiation from the Sun changes on its way to the Earth. The trip the exitance takes before it becomes the irradiance of the Earth is in the vacuum of space where the only thing that can affect its path is a planetary object. Once the radiation reaches Earth and enters the atmosphere, the situation changes and the propagation of light is disrupted by the radiative processes that occur in the Earth's atmosphere. The radiative processes that have a profound effect on the propagation of light in the atmosphere are emission, scattering, and extinction.

The radiative processes account for the disappearance of energy in the atmosphere, energy that is emitted by the Earth and the atmosphere, and the redirection of energy due to reflection and refraction [25]. These processes are illustrated mathematically through the radiative transfer equation, shown in Equation 7, where the total reduced intensity, dI, is found from changes due to extinction, emission, and scattering [25].

$$dI = dI_{ext} + dI_{emit} + dI_{scat} \tag{7}$$

Each component of the equation accounts for reduction in intensity, I, or Blackbody radiation, B, due to each process by utilizing coefficients of extinction (β_e), absorption (β_a), and scattering (β_s).

The extinction piece uses the intensity of the incident radiation along with the atmospheric attenuation coefficient in order to show the the depletion of the intensity. The atmospheric attenuation coefficient, or extinction coefficient shown in Equation 8 [25], can be expressed as the combination of absorption and scattering of light due to gas molecules and aerosols present in the atmosphere [1].

$$\beta_e = \beta_a + \beta_s \tag{8}$$

The emission piece takes into account the Blackbody radiation emitted by both the Earth and its atmosphere. Since Kirchoff's law states a good absorber is a good emitter, the absorption coefficient is used instead of an emission coefficient in order to find the reduction in the Blackbody radiation being emitted by the Earth. The scattering piece, shown in Equation 9, utilizes a phase function, p($\hat{\Omega}'$,$\hat{\Omega}$), the scattering coefficient, and intensity of scattered radiation, $I(\hat{\Omega}')$ [25].

$$\frac{\beta_s}{4\pi}\int_{4\pi} p(\hat{\Omega}', \hat{\Omega}) I(\hat{\Omega}') d\omega' \tag{9}$$

The phase function conveys the probability of light that gets scattered from other directions into the resulting path which is known as multiple scattering. Multiple scattering is defined as the scattering process in which scattering occurs not only with direct solar radiation but also with radiation that has already been scattered off of other aerosols [5]. With the preceding variables, Equation 7 becomes Equation 10 where everything is considered over an infinitesimal distance, ds [25].

$$dI = -\beta_e I ds + \beta_a B ds + \frac{\beta_s}{4\pi}\int_{4\pi} p(\hat{\Omega}', \hat{\Omega}) I(\hat{\Omega}') d\omega' ds \tag{10}$$

Ultimately, the final form of the radiative transfer equation tells us the change in intensity due to a change in optical depth. From Beer's Law, the optical depth or optical thickness, shown in Equation 11, describes the extinction over some infinitesimal distance that is being considered.

$$\tau = \int_{s_1}^{s_2} \beta_e ds \tag{11}$$

The change in optical depth, $d\tau$, is divided through the entire equation and produces a variable called the single scatter albedo, shown in Equation 12, which conveys a ratio of the scattering coefficient to the extinction coefficient.

$$\tilde{\omega} = \frac{\beta_s}{\beta_e} = \frac{\beta_s}{\beta_s + \beta_a} \tag{12}$$

Applying the change in optical depth and single scatter albedo gets the final form of the radiative transfer equation, shown in Equation 13, where the intensity is dependent on the direction of interest, $\hat{\Omega}$ [25].

$$\frac{dI(\hat{\Omega})}{d\tau} = I(\hat{\Omega}) - (1 - \tilde{\omega})B - \frac{\tilde{\omega}}{4\pi}\int_{4\pi} p(\hat{\Omega}', \hat{\Omega}) I(\hat{\Omega}') d\omega' \tag{13}$$

2.3.2 Atmospheric Scattering.

The scattering effects that occur are essentially just reflections in all directions of the radiation off aerosols in the atmosphere. Aerosols are atmospheric particles spanning a wide variety of constituents including dust, organic material, pollutants, ice, water droplets, etc [1]. Aerosols vary in size, shape, distribution, components, and profile concentrations in the atmosphere and they influence the interactions of propagating light in many different ways [1]. The most important thing to consider when discussing aerosol scattering is the comparison between the size of the molecule or particle to the wavelength of light [25]. The comparison can be seen mathematically using the nondimentional parameter given in Equation 14 where r is the *radius of the particle* and λ is the *wavelength* [25].

$$x \equiv \frac{2\pi r}{\lambda} \tag{14}$$

When the particle radius is much smaller than the wavelength, $r <<< \lambda$, light scatters very weakly. When the particle radius is much larger than the wavelength, $r >>> \lambda$, light follows the rules of geometric optics. In between these two extremes, the scattering is explained by either small particle, or Rayleigh, scattering and large particle, or Mie, scattering. Rayleigh scattering is mostly seen when the relation of particle size to wavelength is $r < 0.1\lambda$ and Mie scattering can be seen when it gets to $r \geq 0.3\lambda$ with a transition region of $0.1\lambda \leq r < 0.3\lambda$ between the two regimes [25].

When considering Rayleigh scattering, the two important aspects are the probability that scattering even occurs and the probability scattering at an angle from the original path [25]. First, the angle at which a wave gets scattered could be any angle that exists on the plane that the wave was initially propagating on. The probability of the wave scattering at any angle like in Figure 6a is found with Equation 15 [25].

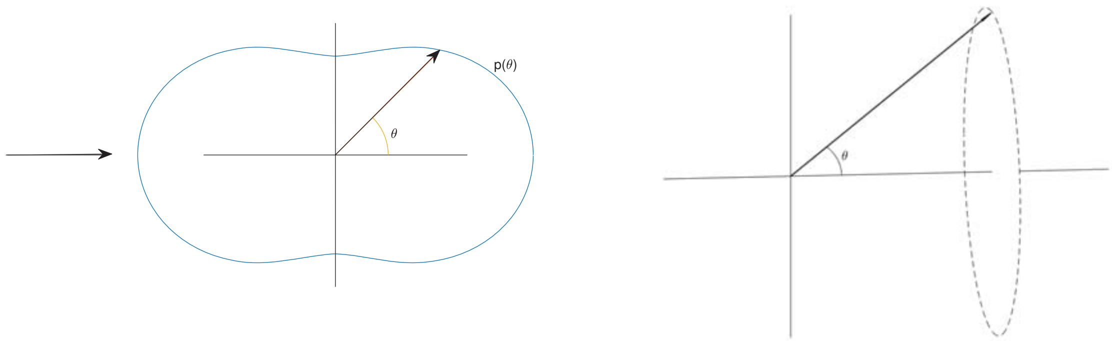

(a) Probability of scattering occurring at any angle

(b) Scattering is dependent only on the angle θ and can occur at any azimuthal angle on the dashed circle

Figure 6. Rayleigh Scattering of radiation in the atmosphere

$$p(\Theta) = \frac{3}{4}(1 + \cos^2 \Theta) \tag{15}$$

Furthermore, Figure 6b conveys that the scattering occurs on the same plane but can occur anywhere on the azimuthal angle about the x-axis. Second, Rayleigh scattering is very dependent on the wavelength of the light that is involved. The probability that the light will even scatter, shown in Equation 16, conveys the proportionality between the wavelength and the Rayleigh scattering cross-section [25].

$$p(\sigma_{RS}) \propto \frac{1}{\lambda^4} \tag{16}$$

The relation between wavelength and scattering cross-section shows us that light at smaller wavelengths scatters more and explains why the sky is blue.

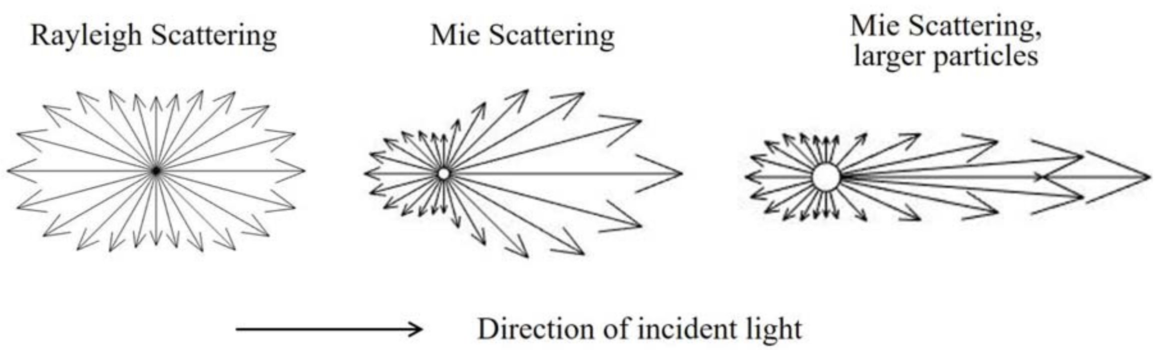

Figure 7. Illustrations of Rayleigh scattering off small particles and Mie scattering off large particles and lager particles

When considering Mie scattering, the shape of the scattering particle is very influential due to the size of the particle and light wavelength being comparable which makes Mie scattering more complicated than Rayleigh scattering [25]. When comparing Rayleigh scattering to Mie scattering, Figure 7 shows for Rayleigh scattering that the likelihood of scattering in all directions is about the same. For Mie scattering, Figure 7 shows that forward scattering dominates more and more as particles get larger.

2.3.3 Atmospheric Absorption.

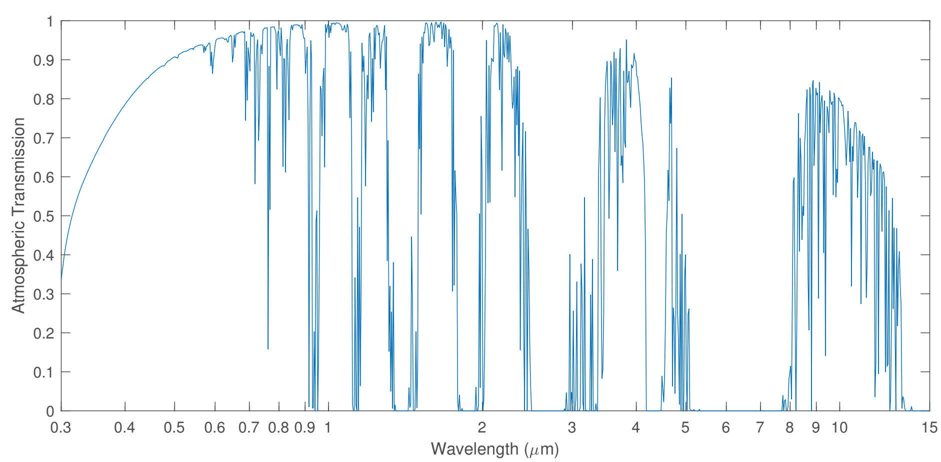

Figure 8. The figure shows how transmission of light is affected by the various constituents present in the atmosphere.

The absorption affects that occur in the atmosphere do so as a result of not only particles that are present but also because of the various gases that make up the atmosphere which is called Continuum absorption. It is referred to as Continuum because the absorbing affects vary smoothly with respect to wavelength and it is divided into three types known as photoionization, photodissociation, and water vapor [25]. The main chemical constituents that contribute to continuum absorption are H_2O, CO_2, O_3, O_2, NH_4, nitrous oxide (N_2O), and carbon monoxide (CO). Every constituent affects the transmittance of light through the atmosphere at different wavelengths mainly in the UV band as well as the IR band and higher wavelengths. The majority of the UV is affected by O_3 while the rest of the chemical constituents contribute to absorption in the NIR and higher wavelengths [25].

Two of the three types of continuum absorption, photoionization and photodissociation, are very well understood while the third, water vapor, is still being discussed [25]. Photoionization occurs when a photon has enough energy to not only excite an electron to a higher state but also enough energy to strip an electron completely which creates a positively charged ion and free electron [25]. Photodissociation occurs when a photon has enough energy that exceeds the chemical binding energy between two components of a molecule [25]. The third and least understood type is the water vapor continuum that primarily affects IR and microwave regions in the EM spectrum. Even though the physical mechanism of the water vapor continuum is not well understood, there are two important things to ultimately remember about it. First, the strength of the continuum is weak in the NIR and thermal IR bands while the strength steadily increases through the far-IR and microwave bands. Second, the volume extinction coefficient, β_e, is not proportional to the water vapor density, ρ_v, but it's more proportional to the square of the density, ρ_v^2 [25].

2.4 Radiative Transfer Code

The final form of the radiative transfer equation shown at the end of Section 2.3.1 is a complex calculation. It needs to take into account absorption, emission, and scattering which effects the intensity of light as it propagates through the atmosphere. One extensive and widely used method for keeping track of the various parameters of the many absorbers in the atmosphere is the HIgh-resolution TRANsmission (HITRAN) molecular absorption database [25]. HITRAN is a compilation of spectroscopic parameters used to predict and simulate the transmission and emission of light in the atmosphere [2]. HITRAN keeps track of the atmospheric effects of the various constituents in the atmosphere at every single wavelength known as absorption line spectra [25]. The massive collection of information associated with HITRAN2016 consists of millions of lines for the different individual wavelengths and 49 different molecular constituents [2].

In an effort to assist with the radiative transfer calculations, radiative transfer codes were developed utilizing different methods including line-by-line calculations, band transmission models, and k-distribution [25]. These methods have different ways of performing the same calculations either by doing them for each wavelength individually or using a group of wavelengths around a central wavelength being examined. While using these methods, LEEDR also relies on boundary layer (BL) processes and aerosol effects modeling to help visualize the radiative processes that occur in the atmosphere.

2.4.1 Boundary Layer Processes in LEEDR.

In part, LEEDR is able to calculate and model atmospheric processes by utilizing the BL processes that are present in the atmosphere. The BL is the lowest level of the atmosphere closest to the Earth's surface that it is not a fixed thickness

[15]. A key characteristic of the BL is that it is well-mixed due to surface heating and cooling that creates turbulence from the induced vertical motions [15]. The surface heating and cooling also causes changes in the height of BL depending on the Time of Day (TOD) and the time of year [14]. LEEDR specifies three BL heights depend-

Table 1. Boundary Layer Heights in Meters Based on Time of Day and Season

Time of Day	Summer	Winter
0000-0259	500	500
0300-0559	500	500
0600-0859	1000	500
0900-1159	1524	1000
1200-1459	1524	1524
1500-1759	1524	1524
1800-2059	1524	1000
2100-2359	1000	500

ing on TOD in three hour increments and two different seasons as seen in Table 1. The summer season is indicated by March through August and the winter season is indicated by September through February [7].

Another characteristic of the BL involves the temperature, shown in Equation 17, which decreases with height at the dry adiabatic lapse rate [11].

$$(\frac{dT}{dz})_{dry} = -\frac{g}{c_p} = -9.8\frac{K}{km} \tag{17}$$

The BL also involves the dewpoint temperature, shown in Equation 18, which is where condensation occurs in a parcel of air cooled at constant pressure [15].

$$(\frac{dT_d}{dz}) = -\frac{g}{\epsilon l_v}\frac{T_d^2}{T} \approx -1.8\frac{K}{km} \tag{18}$$

The dewpoint temperature lapses with height and varies throughout the BL even though the water vapor mixing ratio remains constant [15]. Both temperature equations above convey the change in temperature as the height changes due to a gravitational constant, g, specific heat of air at constant pressure, c_p, the ratio of the molecular weight of water over the molecular weight of dry air, ϵ, and the latent heat (enthalpy) of vaporization of water, l_v. In many cases, saturation can occur within the BL so the lapse rate of temperature is no longer linear with height and decreases at a rate that is less than the dry-adiabatic rate according to Equation 19 [11].

$$(\frac{dT}{dz})_{moist} = -\frac{g}{c_p}\frac{1+\frac{l_v w_s}{RT}}{1+\frac{l_v^2 w_s}{c_p R_v T^2}} \tag{19}$$

All of the variables from Equations 17 and 18 are the same as in Equation 19 with the addition of the saturation mixing ratio of water, w_s, and the moist air gas constant, R_v [15].

LEEDR allows the BL lapse rates to occur on the basis of surface values for an Extreme and Percentile Environmental Reference Tables (ExPERT) site or user-defined surface data [14]. ExPERT is a 30 year climatological database that provides specific site or regional surface and upper air data to characterize correlated molecular absorption, aerosol absorption, and scattering by percentile [10]. A consequence of the lapse rates is relative humidity (RH) varies dramatically in the BL usually from the surface to approximately 100% near the top of the BL [12]. The large variation has a strong effect on aerosol distribution size and strongly affects laser propagation through the atmosphere[14]. The effect is not seen from modeling with standard atmospheric data because the moisture does not lapse realistically in standard atmospheres and RH does not necessarily increase with height in a standard atmosphere BL [12].

2.4.2 Aerosol Effects Modeling in LEEDR.

From earlier discussions on atmospheric processes, aerosols play an important role in the Earth's radiative processes. Aerosols influence the radiation balance through the various optical properties that describe the interaction between aerosols and solar radiation [20]. The optical properties include the absorption coefficient, scattering coefficient, and in turn the extinction coefficient [20]. The properties are wavelength dependent and derived with the help of aerosol size distribution through Mie theory which assumes that particles are spherical and homogenenous [20]. Size distributions for aerosols can be calculated for specific scenarios, locations, altitudes, seasons, and relative humidities [11]. The coefficients are calculated first assuming a dry environment and then allowed to vary with increasing humidity conditions [11].

From those calculations, aerosol models can be created which represent a simple, generalized description of typical atmospheric conditions [20]. Two approaches that define an aerosol model are through direct measurements of the optical properties and computation of the properties with data from different sources[20]. The direct measurements of the optical properties is the most straight forward approach but requires a large number of accurate optical measurements that is not currently available in the required quantity and quality[20]. The computations approach is the only reasonable approach currently available and utilizes aerosol information from Global Aerosol Data Set (GADS) [19] and values derived from the Optical Properties of Aerosols and Clouds (OPAC) [17].

The extinction coefficients mentioned also suggest how the aerosols affect the visibility in the atmosphere. LEEDR calculates visibility at the surface of the Earth as well as visibility along the horizontal or vertical paths [11]. LEEDR also calculates visibility for each of the standard aerosol distributions and allows the user the to specify a surface visibility other than the default value [11]. The OPAC visibility calculation, shown in Equation 20, is accomplished using the aerosol extinction coefficient at 0.55μm, $\beta_{e,0.55}$, and the Rayleigh scattering coefficient at 0.55μm, $\beta_{ray,0.55}$ [11].

$$vis_{OPAC} = \frac{3}{\beta_{e,0.55} + \beta_{ray,0.55}} \tag{20}$$

The path visibility is found considering all absorbtion and scattering effects due to molecules, aerosols, clouds, and rain[11]. The path along which visibility is calculated is divided into a finite number of segments with total extinction in each section added together[11]. The cumulative extinction coefficient is used to get path visibilitiy and surface visibility is obtained from total extinction in the lowest surface segment [11].

2.4.3 Global Aerosol Data Set.

GADS is a worldwide climatological database that describes surface aerosol number densities, size distributions, and optical properties [7]. The radiative properties are calculated using Mie theory for wavelengths between 0.3μm and 40μm considering eight relative humidity values [7]. The atmospheric aerosols generally consist of a mixture of different substances that are influenced by natural and man-made emission, formation, and removal processes [19]. Aerosols are characterized according to 10 primary components, which, in turn, are classified according to characteristic size and wavelength-dependent refractive indices [19].

Typically, aerosols in this data set include water-soluble, water insoluble, soot, sea salt, and minerals where the sea salt particles are defined in two sizes while minerals are defined in four sizes [19]. GADS is set up to describe aerosol properties with mixing ratios depending on season and place with data given for summer and winter months on a global grid with 5°longitude and 5°latitude spacing [19]. The data is consistent with respect to aerosol mass per volume and optical properties that are comparable to different regional and ground based measurements and satellite data along with direct aerosol as radiation observations [19].

III. Methodology

3.1 Overview

The following chapter is a description of the instrumentation used as well as the steps taken in order to obtain the necessary information to correlate LEEDR sky radiance characterizations with actual sky radiance measurements. The chapter is comprised of seven sections that cover the collection of real-time sky radiance measurements, the collection of atmospheric and weather data, and generating sky radiance models. The chapter explains the telescope and spectrometer setup, the atmospheric information LEEDR uses, and how that atmospheric information is set in LEEDR for it to generate simulated sky radiances.

3.2 Experimental Setup and Procedure

3.2.1 Telescope-Spectrometer Setup and Calibration.

In order to investigate the research objectives, the first step is to obtain the real-time sky radiance measurements needed to compare to the simulated LEEDR radiance characterizations. The measured radiances are found using an Ocean Optics QE65000 High-Sensitivity Fiber Optic Spectrometer that is connected to a 16” MEADE LX200 telescope [21]. The spectrometer is a symmetrical crossed Czerny Turner with a 101mm focal length, 14 gratings, and six slit widths. The detector has a 2D arrangement of 1044 horizontal pixels by 64 vertical pixels and is responsive from 200nm to 1100nm (0.2μm to 1.1μm) [24].

The telescope-spectrometer setup is programmed to look at six different positions in the sky and to be able to run all day and night without having to be reset. The six sky positions that measurements are taken correspond to positions of the GEO orbit around the Earth which can be seen in Figure 9 along with sun positions.

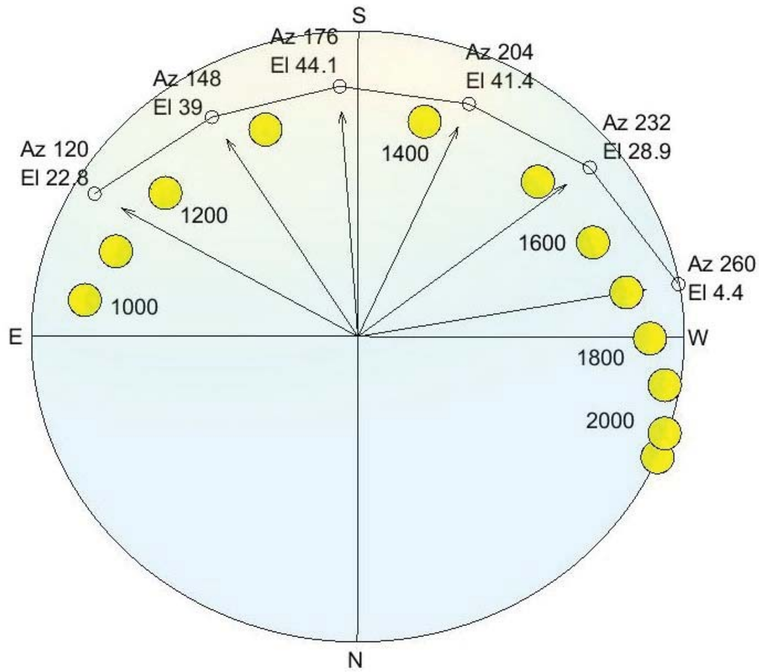

Figure 9. A top down look at sky positions where radiance measurements were taken with average sun positions for the five selected summer days. All times shown are in local Eastern time.

The positions of these points in the sky are indicated by their azimuth and elevation (AzEl) angles. The azimuth angle is the angular position on a horizontal circular plane that is centered around some observer and measured from due North of the Earth. The elevation angle is the angular position in the vertical direction measured up from the same horizontal circular plane.

Table 2. Specific Angles Corresponding to the Six Sky Positions

Azimuth	Elevation	Zenith
120°	22.8°	67.2°
148°	39°	51°
176°	44.1°	45.9°
204°	41.4°	48.6°
232°	28.9°	61.1°
260°	4.4°	85.6°

A list of the AzEls with the corresponding zenith angles for that particular elevation can be seen in Table 2. The zenith angle is the angular position measured down towards the horizontal plane from a 90°elevation angle. The program starts at 120°azimuth and proceeds to take sky radiance measurements at each position moving back and forth in the sky from 120°to 260°for the desired time that measurements are taken.

The sky radiance measurements that are considered herein are for five clear or nearly clear days in May, June, and August. The choice of days and times is based on having the necessary atmospheric and weather information available. The times being compared for each day are separated by at least an hour or more in order to have a definitive difference in atmospheric and weather conditions for each time. The spectrometer takes intensity measurements in counts while utilizing several different integration times just like exposure times in a camera. The integration time is selected to be the same for all times and the highest integration time before saturation occurred.

After the integration time is chosen, the data collected needs to be calibrated due to the spectrometer reading the sky brightness as a digital number. The spectrometer readings are put through a two-point calibration method using a distant star as the source for the radiance calibration. The telescope and spectrometer are used to measure the radiance of the star that reaches Earth as well as a measurement with the lens cap on for the darkness to use as a zero point. The radiance of the star and darkness are also calculated using Planck's Blackbody equation to use as a second point for the calibration.

The calculated radiances for the star, L_2, and the dark, L_1, as well as the spectrometer measurements of the star, N_2, and with the lens cap on, N_2, are used to get a gain and an offset shown in Equation 21 and Equation 22 respectively.

$$g = \frac{N_2 - N_1}{L_2 - L_1} \tag{21}$$

$$d = \frac{L_2 N_1 - L_1 N_2}{L_2 - L_1} \tag{22}$$

The gain and offset from Equations 21 and 22 are then used to get the actual radiance values corresponding to the spectrometer sky measurements by using Equation 23.

$$L = \frac{N - d}{g} \tag{23}$$

The spectrometer used for the measurements utilizes a wavelength range of $619.5nm$ to $984.5nm$ ($0.6195\mu m$ to $0.9845\mu m$) necessitating all radiance calculations to be done over those same wavelengths.

3.2.2 Observed Meteorological Data.

Obtaining radiance characterizations from LEEDR requires atmospheric inputs for the radiative transfer equation. The first set of atmospheric inputs that are used to obtain radiance simulations in LEEDR are the three observed surface MET parameters, or MET data, of pressure, air temperature, and dew point. The MET data is the easiest to obtain since it is constantly tracked everyday at various time intervals ranging from every minute to upwards of every hour. The MET data obtained for this research is found using a Vantage Pro 2 console connected to a weather observation station [8]. The MET data is recorded in Coordinated Universal Time (UTC) at intervals of every minute. Since spectrometer measurements are recorded to the second, the MET data is interpolated in order to also get values down to the second for the same days and times being investigated.

3.2.3 Real-Time Aerosol Particle Concentrations.

The next atmospheric input necessary for this research, and one of the most important, is the aerosol particle concentration or particle counts in the atmosphere.

The particle concentrations for the area over the telescope were found using two types of Condensation Particle Counter (CPC). Model 3788 Nano Water-Based CPC and Model 3800 Kanomax Alcohol-Based CPC are able to report particle sizes, particle concentrations, and aerosol flow rate. The water-based model was the main CPC used and the alcohol-based model was utilized as a backup when the water-based was unavailable due to maintenance, recalibration, etc. For the five days that were investigated, the water-based model was used on four days while the alcohol-based was used on one day.

The water-based CPC is able to count particles in the atmosphere ranging in sizes from 2.5nm and upwards of $3\mu m$ [27]. It can also measure total aerosol concentrations up to around $4x10^6\frac{particles}{cm^3}$ with an aerosol flow rate of $0.3\frac{L}{min}$ [27]. The alcohol-based CPC is able to count particles in the atmosphere ranging in sizes from 15nm and upwards of $1\mu m$ [18]. It can also measure total aerosol concentrations up to around $0.1x10^6\frac{particles}{cm^3}$ with an aerosol flow rate of $0.1\frac{L}{min}$ [18].

The particle counts are extremely important to have since the number of particles in the atmosphere directly affects how much radiance is actually detected. LEEDR is able to closely match measured radiances by utilizing climatological GADS information. GADS deduces the particle concentrations for Wright-Patterson Air Force Base (WPAFB) to be 28,200 $\frac{particles}{cm^3}$. However, recent research shows that diurnal aerosol concentrations actually vary throughout the day and also from day to day as can be seen in Figure 10 [13]. Even though LEEDR can come close with climatological GADS information, the variations in diurnal concentraions means it fails to accurately predict the values without real-time observations.

Accurate radiance models are accomplished by obtaining reported visibility conditions to match aerosol loading to the real-time atmospheric conditions [6]. Visibility conditions can be matched by scaling the BL extinction coefficient but that does not

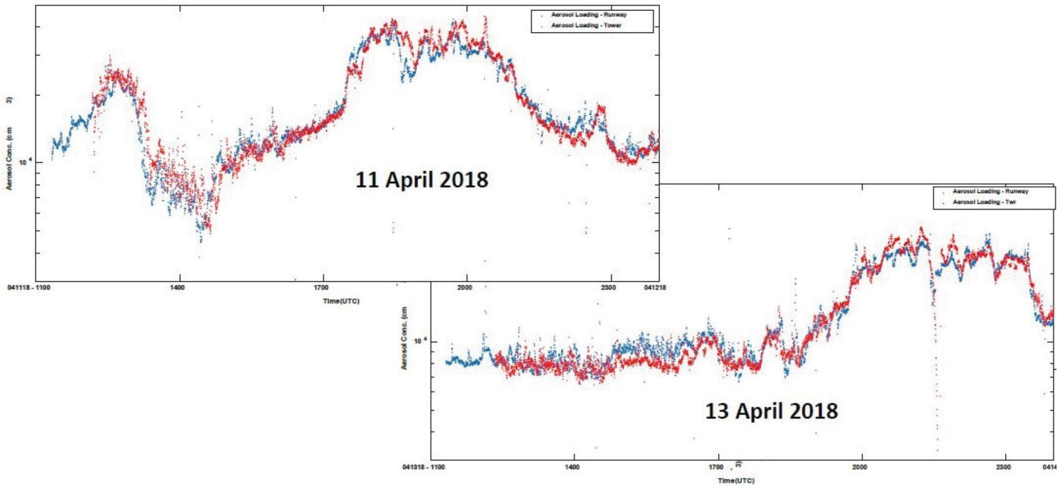

Figure 10. Diurnal particle concentrations over time for two different days at Wright Patterson AFB [13]

account for scaled aerosol effects at other atmospheric layers [6]. A more accurate way is to alter the climatological surface aerosol information obtained from GADS until calculated visibility matches the observed [6]. In order for LEEDR to use the number of particles counted in the atmosphere to make radiance calculations, it must first scale the embedded climatological GADS values to correspond to the actual aerosol measurements.

LEEDR implements an aerosol multiplier which scales the climatological information associated with GADS. The default multiplier in LEEDR is set to one and means the particle counts are the same as the GADS seasonal climatological total surface number concentration of 28,200 $\frac{particles}{cm^3}$. Once the number of particles for the given day and time are measured, the measured particle counts are divided by the climatological surface number concentration associated with the GADS aerosol climatology for that day and time [7]. The scaled multiplier for the specific days and times is what LEEDR uses to simulate the path radiance of the atmosphere for those same days and times.

3.2.4 Numerical Weather Prediction.

The last input that is focused on is NWP data found by using the National Oceanic and Atmospheric Administration (NOAA) Global Forecast System (GFS). The GFS is a weather forecast model produced by the National Centers for Environmental Prediction (NCEP) that couples four separate models covering atmosphere, ocean, land/soil, and sea ice [22]. Many variables are covered by GFS due to the combined four models and include but are not limited to temperature, wind, precipitation, soil moisture, and atmospheric ozone concentration [22]. The GFS is used to predict weather up to 16 days in the future and covers the entire globe at a base horizontal resolution of 28km between grid points [22]. When the forecasts are between one and two weeks out, the horizontal resolution drops to 70km between grid points [22].

Before LEEDR assessments can be made using the forecasts from GFS, it is necessary to determine which forecast should be used for the specific times and days that are considered. The GFS model chosen for this research lays out the Earth in a 720 by 361 grid with each grid point at 0.5°. It produces four forecast cycles per day at 0000, 0600, 1200, and 1800 hours in UTC with output time steps for each cycle of three hours ranging from 0 hours to 192 hours [22]. The GFS data LEEDR uses is pulled from the NOAA Operational Model Archive and Distribution System (NOMADS). NOMADS is a repository of weather model output datasets, model input datasets, and a limited subset of climate model datasets generated by NOAA [23]. The National Centers for Environmental Information (NCEI) provides near-real-time access to these weather model forecast data in addition to historical model data. The GFS data for this research is either a six hour or a nine hour forecast that is closest to whatever time is being examined.

3.2.5 Laser Environmental Effects Definition and Reference.

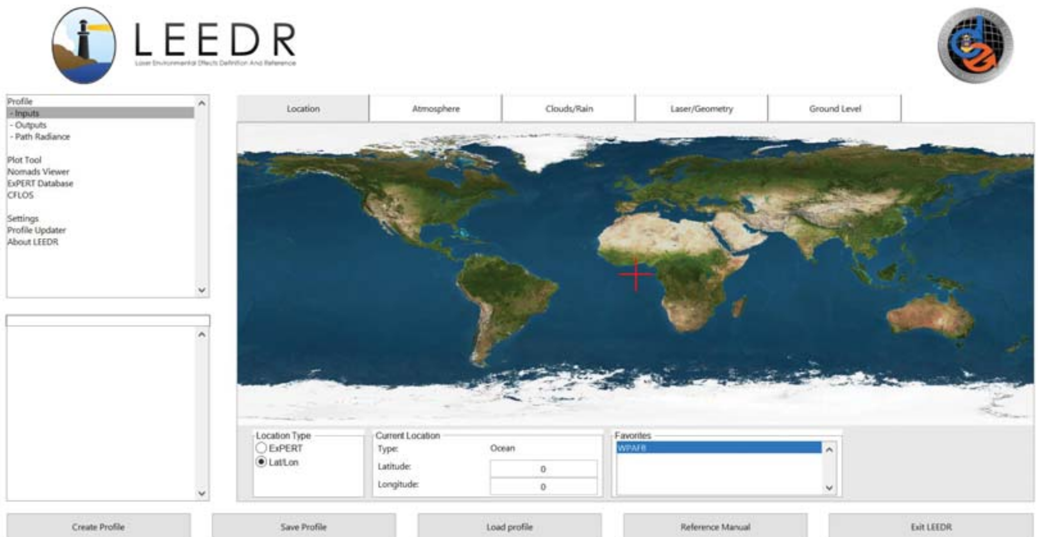

Figure 11. Laser Environmental Effects Definition and Reference

The assessment of the accuracy of LEEDR compared to the real-time radiance measurements already obtained now requires radiance simulations from LEEDR. LEEDR demonstrates the ability to come close to measured values using realistic atmospheric information from ExPERT and GADS [6]. However, LEEDR fails to accurately predict actual radiance measurements without atmospheric information from weather observation stations, CPC, or NWP. In order to increase the accuracy of LEEDR simulations, the atmospheric information from these sources must be used.

Once all of the preceding atmospheric information is compiled, LEEDR is used to generate radiance simulations based off that information. Initially, LEEDR version 4.00.026 was used with the intention of creating seven simulations a piece for 47 days and times along with all six sky positions for each time for a total of 8,742 simulation. After the release of version 4.00.027, the same procedure was continued with the newer version and half the radiance simulations were collected. Once version 4.00.027.1 was released, an inspection of the radiance simulations between the three versions reveals radiance characterizations from version 4.00.027 were inaccurate. The inaccuracies in the collected simulations forced a restart of the data collection and a revision in the initial procedure to accommodate a reduced time frame in data collection

The revised and final plans was to use version 4.00.027.1 to generate 31 simulations for each of the 24 days, times, and sky positions to get a total of 744 simulations. The days and times were chosen so that all of them had particle counts available and any unexpected weather change wasa avoided. Times and sky positions were randomly paired together and those pairs were randomly chosen for each day keeping in mind atmospheric data availability and weather. Even though version 4.00.028 was released during implementation of the revised plan, a spot check showed no significant change in radiance values and the remaining data collection was completed with version 4.00.028.

The three sets of inputs needed to be configured in LEEDR are the ones that apply to all simulations, the inputs that represent sun and sky position, and finally the specific atmospheric inputs. The inputs that apply to all generated simulations include the location being looked at, wavelength range being examined, number of atmospheric layers considered, etc. The position inputs include date and time in UTC for the sun position as well as the azimuth and zenith angles of the sky position being observed. Finally, the atmospheric inputs are those specific values for pressure, air temperature, dew point, aerosol concentrations, and NWP data that correspond to whatever specific day and time is being examined.

The first thing that needed to be accomplished in the LEEDR GUI was to apply the inputs that are used for every LEEDR generated simulation which can be seen in Table 3. The inputs include the location and atmospheric layers on the Inputs page as well as wavelength, surface, and path information on the Path Radiance page. The local ExPERT site was chosen in order to apply the accurate surface and atmospheric data for absorption and scattering. The atmospheric layers were set so the resolution

Table 3. **General Unchanging Inputs Set in LEEDR for all Radiance Simulations**

Inputs Page			
Locations Tab			
Location Type	ExPERT	**Favorites**	WPAFB
Atmosphere Tab			
	Settings	1000 Layers	
Path Radiance Page			
Inputs Tab			
Wavelength (m)	3.5e-07 to 1e-06	**Molecular Points**	1000
Use Multi-Scatter	Checked	**Surface Temperature (K)**	300
Path Altitude (m)	1	**Path Resolution**	200

of the atmospheric profile was 100m based on a full atmosphere of 100km. Next, the wavelength range was set for the visible to NIR with a variation of 1000 total wavelengths and multi-scatter principles were applied to all radiance models. Finally, a typical surface temperature of the Earth was set, the height was configured for a ground observer, and a resolution was set to indicate 500 meter layers in a 100km atmosphere.

Once all of those inputs were set, LEEDR could be used to generate plots based on the specific times, days, sky positions, and atmospheric information. For this, the date, time, and sky position should be selected on the Path Radiance page for the specific instance being investigated. The date is specified by using the calendar and the specific hour, minutes, and seconds in UTC are set below that. The sky position is then chosen by inputting the zenith angle in degrees and the azimuth angle in degrees. The final step in generating radiance simulations is providing the specific atmospheric inputs for the time and day being investigated. The surface MET observations are entered in the Ground Level tab while the ExPERT, NOMADS, and GADS information are all set in the Atmosphere tab. A total of 31 Profiles were created for each of those inputs as well as all combinations of those inputs and all 31 combinations can be seen in Table 4.

The first group is seven input combinations for the three MET observations

Table 4. The Four Groups of 31 Atmospheric Input Combinations

MET Obs	Particle Obs	NWP	Particle Obs w/ NWP
Pressure	Particles	NWP	Particles NWP
Air Temperature	Parts Press	NWP Press	Parts NWP Press
Dew Point	Parts Temp	NWP Temp	Parts NWP Temp
Press Temp	Parts Dew	NWP Dew	Parts NWP Dew
Press Dew	Parts Press Temp	NWP Press Temp	Parts NWP Press Temp
Temp Dew	Parts Press Dew	NWP Press Dew	Parts NWP Press Dew
MET Obs	Parts Temp Dew	NWP Temp Dew	Parts NWP Temp Dew
	Parts MET Obs	NWP MET Obs	Parts NWP MET Obs
Press - Pressure Temp - Air Temperature Dew - Dew Point			
MET Obs - Press/Temp/Dew combined Parts - Measured Particles			

and all three of them together. The next group is eight input combinations for the measured surface aerosol information alone and with the seven MET combinations. The third group is eight input combinations for the NWP data alone and with the seven MET combinations. The final group is eight input combinations for measured aerosols with NWP data alone and both with and the seven MET combinations. The MET and Particle groups both use ExPERT information while the NWP and Particle with NWP groups both use information from NOMADS. Also, the MET and NWP groups use climatological aerosol information while the Particle and Particle with NWP groups both use measured aerosol information.

3.2.6 Spectral Sky Radiance Modeling.

After the inputs from Table 4 are entered into LEEDR, a specific profile was created by pressing the Create Profile button at the bottom of the LEEDR GUI. After a profile ascreated, a sky radiance characterization was generated by pressing the Calculate button towards the bottom of the Path Radiance page. Once generated, the radiances for a characterization were saved in an excel file by pressing the Save button under the radiance plot. The 31 simulations that cover all combinations of atmospheric and weather inputs were done for all 24 specific days, times, and sky positions.

The ExPERT information needed for profiles was chosen by selecting the appropriate season and three hour TOD in local time below the drop down in the Atmosphere section that has ExPERT selected. The NOMADS information needed for profiles was chosen by selecting NOMADS from the Atmosphere section drop down and then the appropriate date, cycle, and time in UTC. The GADS information needed for profiles was chosen by changing the multiplier below the drop down with GADS selected in the Aerosols section. Climatological GADS information was indicated by leaving the multiplier at one and measured aerosol information was indicated by changing the multiplier to the scaled factor for the corresponding measured aerosol concentration.

For the profiles of MET observations, the ExPERT and climatological GADS information was applied and profiles were made for only pressure, only air temperature, etc. For the profiles of particle observations, the ExPERT information was applied and the aerosol Multiplier was changed to the scale factor for the measured aerosol concentration. Following that, profiles were made for measured aerosols alone, measured aerosols with only pressure, measured aerosols with only air temperature, etc. For the profiles of NWP data, the NOMADS and climatological GADS information was applied and profiles were made for NWP data alone, NWP with only pressure, NWP with only air temperature, etc. For the profiles of particle observations with NWP data, the NOMADS information and the scaled multiplier was applied. Following that, profiles were made for measured aerosols with NWP data alone followed by both with only pressure, both with only air temperature, etc.

Once all 744 simulations were obtained from LEEDR with the atmospheric information, one more simulation was done for each of the 24 times. In order to properly show how the accuracy of LEEDR changes with information, a profile was made using only information from ExPERT and climatological information from GADS. The simulation from this combination provides a proper picture of how LEEDR begins to characterize spectral sky radiance on its own. From there, the picture became even clearer when all simulations were put together to find out how much radiance each atmospheric input helps simulate.

IV. Results and Analysis

4.1 Overview

The following chapter is intended to present and analyze the results of the comparisons that were made between the measured data and the simulated data obtained using LEEDR. It was hypothesized the best approach is coupling surface MET observations of pressure, air temperature, and dew point with surface aerosol particle concentrations. The first objective was to test the accuracy of LEEDR radiance characterizations while using surface MET observations and climatological aerosol information from GADS. Objective two was to further determine the accuracy of LEEDR while using only NWP data with climatological GADS information alone and measured surface aerosol information alone. The final objective was to see how accurate LEEDR is while coupling surface MET observations, climatological or measured aerosol information, and NWP data.

4.2 Radiance Model Comparison

In the process of investigating the problem at hand, a number of issues were discovered that play a huge role in getting accurate results. The issues have to do with not only the atmospheric inputs that go into LEEDR but also considerations that affect the measured data as well. First, when obtaining the actual radiance measurements for certain days, times, and sky positions, the calibration is the key process that produces accurate results. Second, when using LEEDR to produce the numerous radiance models, it is absolutely imperative to have all of the necessary atmospheric inputs and days, times, and sky positions. Finally, when looking to get accurate radiance characterizations, the choice of days and times is important because atmospheric information may not always be available to use.

4.2.1 Time and Day Choice and Radiance Measurement Calibration.

The ultimate decision of what combination of days, times, and sky positions comes down to ensuring a broad sample of possible combinations that all had the necessary atmospheric information available to use. The days and times chosen all had spectral sky radiance measurements and surface aerosol concentration measurements available. Nearly all of the days and times were clear or nearly clear sunny days with no clouds present ensuring the desired aerosol-only scatter effects.

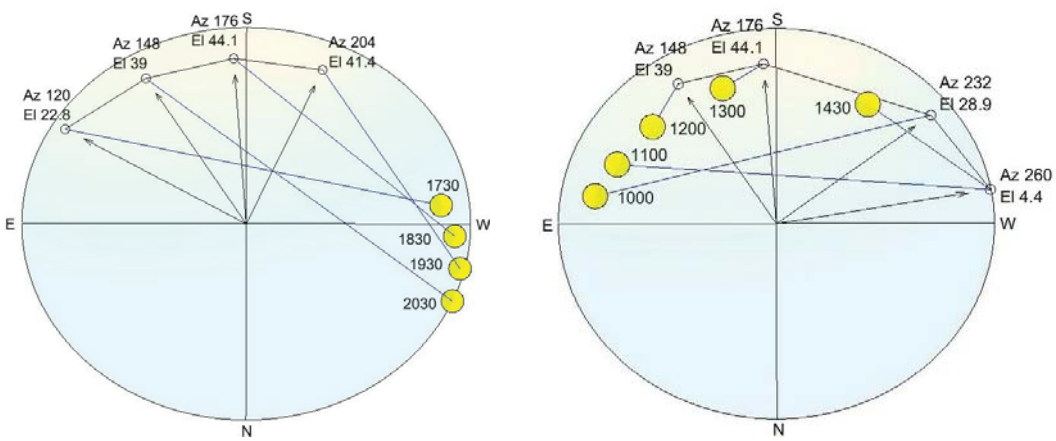

(a) 10 May 2018 (b) 11 May 2018

Figure 12. Sky and Sun positions chosen for May 2018 where the blue lines indicate the sky position that was examined at that time of the day. All times are shown in local Eastern time.

The first time and sky position combinations, shown in Figure 12, are on 10 May from 1730 to 2030 local time at every hour and on 11 May from 1000 to 1300 local time every hour and additionally at 1430 local time. The blue lines in each figure indicate the location in the sky the telescope/spectrometer setup was pointing for each time on the designated day. Real-time radiance measurements were not available before 1730 on 10 May and particle counts were unavailable after 1430 on 11 May.

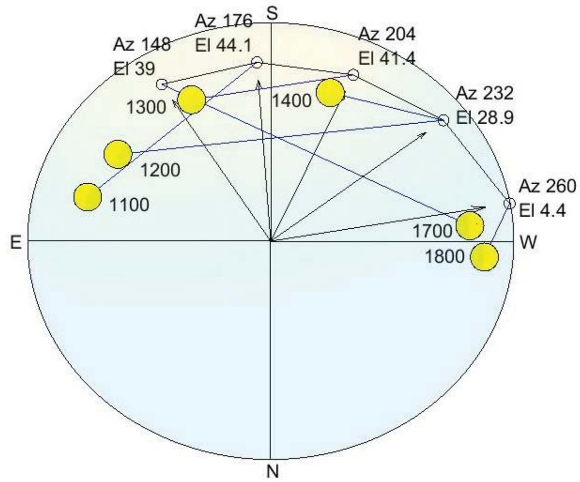

Figure 13. Sky and Sun positions chosen for 15 June 2018 where the blue lines indicate the sky position that was examined at that time of the day. All times are shown in local Eastern time.

The next time and sky position combinations, shown in Figure 13, were chosen for 15 June from 1100 to 1400 local time every hour as well as 1700 and 1800 local time. While real-time sky radiance measurements were available all day from midnight to midnight, the necessary particle counts were only available for the times chosen.

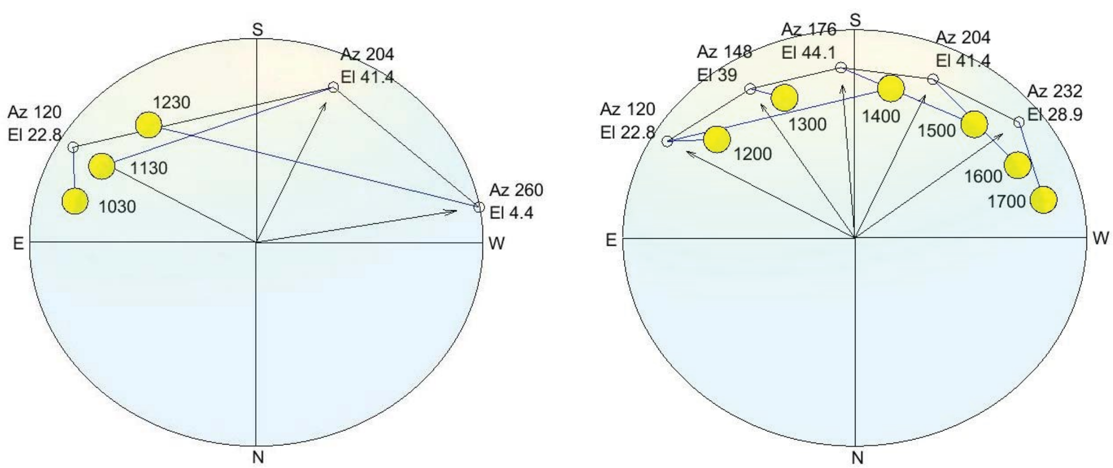

(a) 2 August 2018

(b) 3 August 2018

Figure 14. Sky and Sun positions chosen for August 2018 where the blue lines indicate the sky position that was examined at that time of the day. All times are shown in local Eastern time.

The final time and sky position combinations, shown in Figure 14, are for 2 August from 1030 to 1230 local time every hour and for 3 August from 1200 to 1700 local time every hour. The choice for times on 2 August was limited due to cloudy skies before 1030 and particle counts were unavailable after 1230 and the choice for times on 3 August was limited before 1200 due to cloudy skies.

Before comparisons can be made between measured radiances and LEEDR generated radiances, the measured radiances need to be calibrated from the raw spectrometer data into actual sky radiance values requiring a selection of integration time for all time and sky position combination. The choice of which integration time was

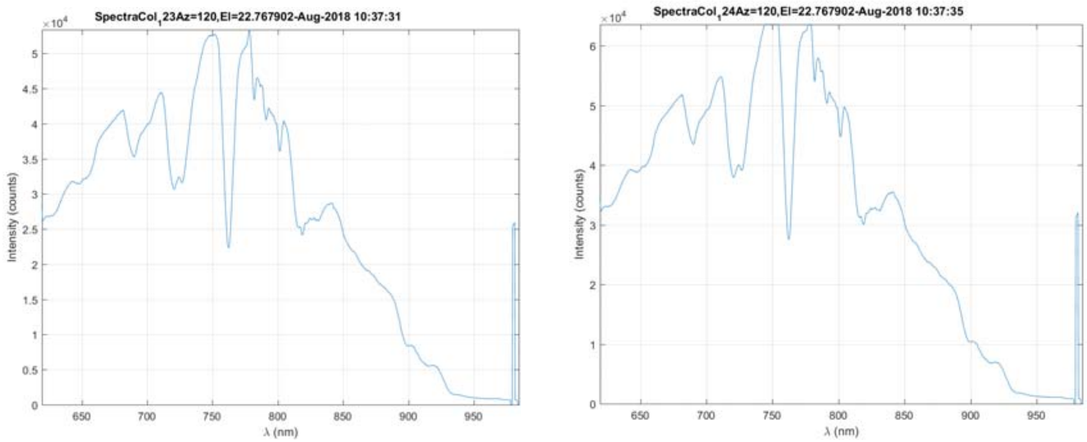

(a) Unsaturated and uncalibrated brightness at integration time of 12000μs

(b) Saturated and uncalibrated brightness at integration time of 15000μs

Figure 15. Raw spectrometer data for 2 August at 1030

decided by looking at the available integration times for all 24 instances and finding the highest integration without saturation occurring. The approach is illustrated in Figure 15 which shows raw spectrometer data at 1030 on 2 August at an integration time of 12000μs (15a) and an integration time of 15000μs (15b).

The threshold value for an integration time to be saturated is when the digital number of the brightness is measured to be 60000 counts or more. Figure 15 shows the highest counts at 15000μs are higher than the threshold and the next lower integration time is shown to be under the threshold. When done for all days/times/AzEls, the lowest useable integration times for 10 May, 11 May, 15 June, 2 August, and 3 August are respectively 40000μs, 20000μs, 20000μs, 12000μs, 20000μs. The best choice of integration time for radiance comparison for all days being examined was chosen to be the 12000μs.

4.2.2 LEEDR Path Radiance Outputs and Analyisis.

Once calibration was completed on the measured radiance data, plots were made in order to compare them with the times and sky position combinations. Figure 16 shows the times and sky positions next to the plot of the sky radiance measurements for 3 August. In Figure 16b, the legend from top to bottom corresponds to the plots as well from top to bottom.

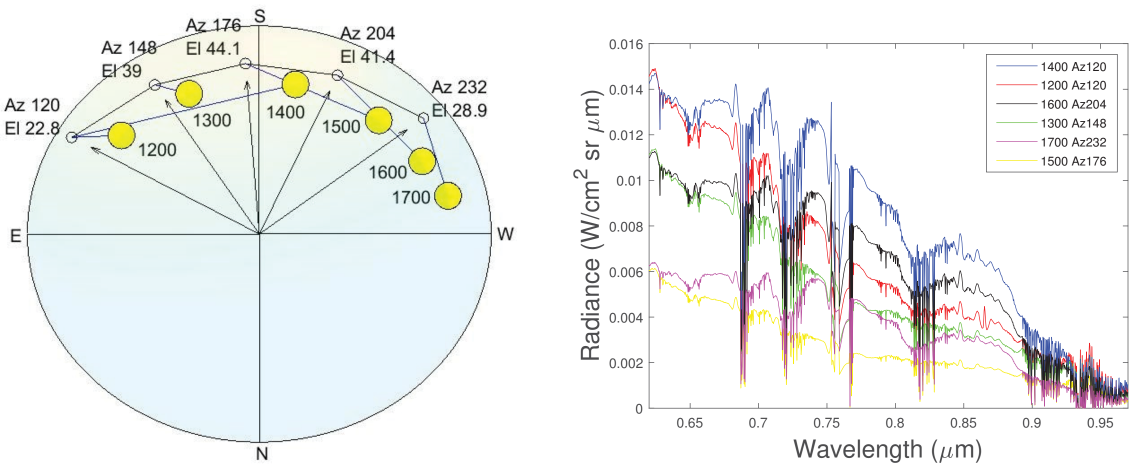

(a) Times and sky position combinations (b) Calibrated measured sky radiances

Figure 16. Times and Sky Positions with Sky Radiances for 3 August

The next set of radiance plots created is a combined plot with all 31 LEEDR radiance simulations, climatological simulation, and the measured sky radiances for all 24 day, time, and sky position combinations. The purpose with combining every plot together is to get a general idea of where the radiances are for each of the 24 combinations. Figure 17 shows all simulated and measured radiances for an AzEl of 204°-48.6°on 3 August at 1600. Figure 17 also shows areas of the plots that were determined to be the areas to use for comparing LEEDR radiances to the measured radiances. In order to make comparisons, it was decided that utilizing the same stable trends in all of the radiance plots would simplify the analysis.

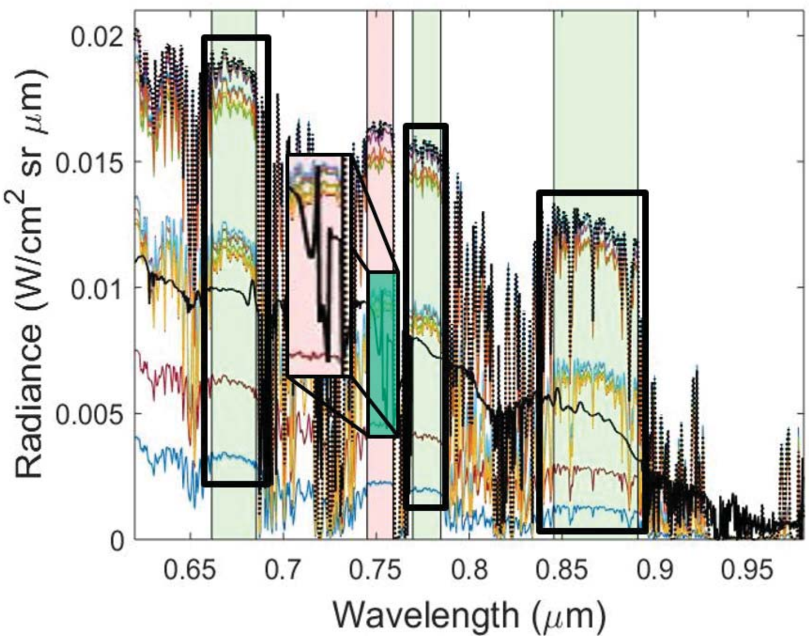

Figure 17. Example of the combined radiance plots of all LEEDR simulations in color along with the plot of the measured values in black and climatological simulation in dotted black for the day/time/AzEl of 204°-48.6°on 3 August at 1600.

When examining the plots, it is easy to see the majority of wavelengths have unstable trends in the radiance values except four sections. The green sections between wavelengths 0.6615μm-0.6853μm, 0.7703μm-0.7847μm, and 0.8456μm-0.8907μm can be seen to have the most stable trends in all LEEDR simulations and measured radiances. The one red section between wavelengths 0.7451μm-0.7591μm shows that the LEEDR radiances have stable trends but the measured radiances do not for that area. When looking at all 24 day, time, and sky position combinations, the same four stable trends can be seen in all of the simulated and measured radiance plots.

While examining the combined radiance plots, the next observation made for all of the LEEDR radiance simulations is they tend to group together with clear separations. In Figure 18, the groupings are circled for LEEDR radiance plots on 3 August at 1600 local time. After looking at all 24 days and times, all of them have similar grouping trends with their LEEDR plots. The number of groupings and the separation between the groups varies for all 24 times but each one has the same grouping trend.

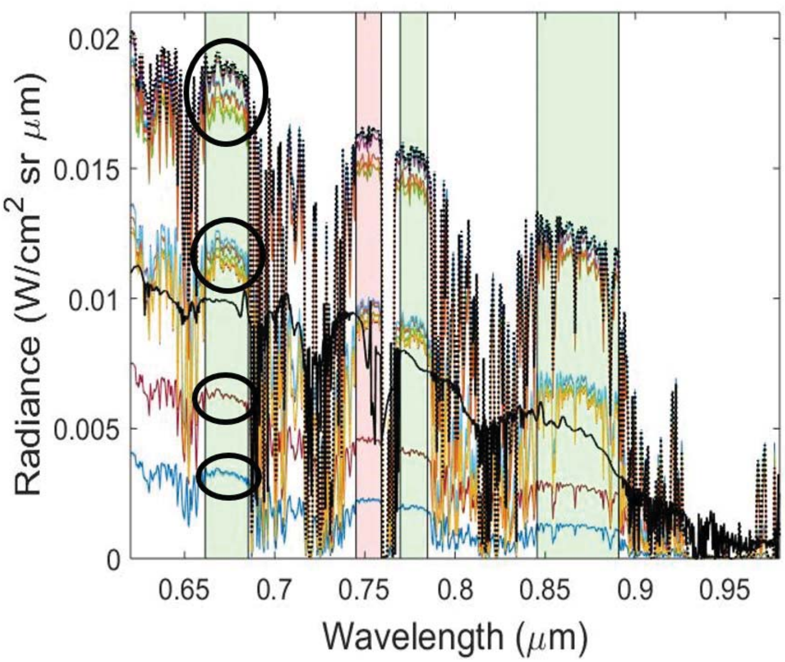

Figure 18. The example here of 3 August at 1600 local time illustrates how all days and times have varying separations between varying groupings of the simulations

The grouping of the simulations led to further investigation into identifying which inputs are producing which radiance simulations. The radiance values for the wavelengths of the green sections are extracted from the data and an average radiance over all wavelengths was found for each simulation. The same average over all wavelengths for each simulation was accomplished for each 24 days and times in question. After that, another average was determined for each simulation over all 24 days and times in order to get one over all average radiance for each simulation.

The averages were used to get a ranking of simulated radiances from highest radiance values to lowest radiance values. The ranking provides a general idea of how much radiance LEEDR is simulating due to each of the 31 atmospheric input combinations and the climatological simulation. Table 5 shows the ranking described and also shows an interesting trend involving the input groupings previously shown in Table 4. If you look closely at Table 5, the input groups from Table 4 tend to produce

Table 5. General Radiance Hierarchy for all 24 Day, Time, Sky Position Combinations

1. Dew Point	12. Parts Dew	23. NWP Press Dew
2. Press Dew	13. Parts Press	24. NWP
3. Climatological	14. Particles	25. NWP Temp
4. Pressure	15. Parts Press Temp	26. NWP Dew
5. Air Temperature	16. Parts Temp	27. Parts NWP Press
6. Press Temp	17. Parts MET Obs	28. Parts NWP Press Temp
7. Temp Dew	18. Parts NWP MET Obs	29. Parts NWP Press Dew
8. MET Obs	19. Parts NWP Temp Dew	30. Particles NWP
9. NWP Temp Dew	20. Parts Temp Dew	31. Parts NWP Temp
10. NWP MET Obs	21. NWP Press	32. Parts NWP Dew
11. Parts Press Dew	22. NWP Press Temp	
Press - Pressure Temp - Air Temperature Dew - Dew Point		
MET Obs - Press/Temp/Dew combined Parts - Measured Particles		

radiance simulations in the same four hierarchical levels. In Table 5, numbers 1-8 are all the MET observations with ExPERT and climatological GADS information. Numbers 11-17 and 20 are all measured aerosol information with ExPERT information and MET observations. Numbers 21-26 are all NWP data with climatological GADS information and MET observations. Numbers 27-32 are all measured aerosol information, NWP data, and MET observations.

Table 5 shows that LEEDR simulates different levels of sky radiance depending on what atmospheric information it is using. In general, LEEDR simulates the highest radiances when it is relying on ExPERT and climatological GADS information with some MET observation(s). The amount of radiance simulated by LEEDR drops when it is given measured aerosol information instead of climatological GADS information. The simulated radiance is even lower when LEEDR uses NWP data instead of ExPERT information along with climatological GADS information and MET observation(s). The lowest simulated radiances by LEEDR come when it is using measured aerosol information and NWP data along with MET observation(s). The two exceptions to this four level radiance hierarchy are numbers 9 and 10 as well as 18 and 19 which are simulating higher radiances than their corresponding groups. The common features of these specific input combinations are that all four use an air temperature and a dew point to simulate radiances.

The next thing that needs to be investigated is the comparison between all of the LEEDR characterizations and the measured radiance values. The analysis accomplished for the comparison between all of the LEEDR characterizations and the measured data simply comes down to finding the differences between them. The radiance values for the green sections of the plots were extracted from the data and differences were found at each wavelength between the LEEDR radiances and the measured radiances. An average difference was then found over all wavelengths for all LEEDR characterize for each of the 24 days and times in question. From those average differences, an average difference over all days and times was found for all 31 input combinations. With those overall averages, the smallest average radiance differences supply the input combinations that produce the most accurate radiance values as depicted in Table 6.

Table 6. 15 Most Accurate Input Combinations Over all 24 Days & Times

1. Parts NWP Press	6. NWP Press Temp	11. NWP
2. Parts NWP Press Temp	7. NWP Dew	12. Parts NWP Dew
3. Parts NWP Press Dew	8. NWP Temp	13. Parts Temp Dew
4. Particles NWP	9. NWP Press Dew	14. Parts MET Obs
5. Parts NWP Temp	10. NWP Press	15. Parts NWP Temp Dew
Press - Pressure Temp - Air Temperature Dew - Dew Point		
MET Obs - Press/Temp/Dew combined Parts - Measured Particles		

A closer inspection of Table 6 shows a clear usage of specific atmospheric and weather inputs in getting accurate radiance characterizations. All but two of the top 15 combinations utilize NWP data to get accurate radiance characterizations and the five most accurate combinations also utilizes measured aerosol information. The pressure, air temperature, and dew point are all used in most of the combinations and their usage is more random when determining accurate radiance values. Pressure is a common input used in the top three accurate combinations but that is unexpected since the air temperature and dew point are more directly related to changes in sky radiance.

When considering the NWP combinations, NWP and NWP with measured particles are considered different from those that also utilize MET observations. The difference is based on what surface information LEEDR allows to be used for the BL lapse rates. When NWP data is used without MET observations, LEEDR applies the predicted surface values for the lapse rates throughout the entire atmosphere. When any combination of MET observations are applied in the Ground Level tab, LEEDR forces the user-defined surface information to be applied throughout the BL. From there, LEEDR applies the default numerical prediction above the BL throughout the rest of the atmosphere. Furthermore, a consequence of the lapse rates with MET observations is that the RH varies dramatically within the BL. The same variation is not seen when utilizing NWP because the moisture does not lapse realistically.

Further inspection into the individual input statistics for accurate simulations reinforces the initial analysis of which inputs are important. The amount of times each input was used for the most accurate combinations was determined by looking at the most accurate combinations in each of the 24 days and times. The total amount each individual input was used in the 15 most accurate combinations for each time was found to see which inputs were used the most in the most accurate combinations.

Table 7. Percentage an Input was Used in the 15 Most Accurate Combinations of all 24 Times

Inputs	10 May	11 May	15 June	2 August	3 August	Overall
Pressure	46.67	52	48.89	53.33	48.89	49.72
Air Temperature	48.33	49.33	50	55.56	45.56	49.17
Dew Point	65	40	48.89	57.78	41.11	48.89
Measured Particles	65	54.67	60	55.56	57.78	58.61
NWP & MET Obs	60	62.67	63.33	40	56.67	58.06
NWP	10	10.67	11.11	2.22	10	9.44
Note: Statistics reflect usage of just the individual input mentioned and not ExPERT or climatological GADS information usage						

Table 7 shows the percentage each input was used for each day as well as how much they were used overall. In general, it can be seen that the NWP data, scaled GADS aerosols, and MET observations were used the most in order to get the most accurate radiance values. The pressure, air temperature, and dew point are all used slightly less and not one of the MET observations are used more than the others. If the scope of individual input usage is narrowed to the 10 most accurate combinations (Table 8) and the five most accurate combinations (Table 9), similar results are found to those of the 15 most accurate combinations.

Table 8. Percentage an Input was Used in the 10 Most Accurate Combinations of all 24 Times

Inputs	10 May	11 May	15 June	2 August	3 August	Overall
Pressure	45	52	48.33	50	46.67	48.33
Air Temperature	60	40	48.33	53.33	35	45.83
Dew Point	62.5	38	53.33	46.67	41.67	47.92
Measured Particles	75	44	73.33	63.33	60	62.92
NWP & MET Obs	65	76	60	30	56.67	59.58
NWP	10	12	10	3.33	13.33	10.42
Note: Statistics reflect usage of just the individual input mentioned and not ExPERT or climatological GADS information usage						

One final observation to look at is on 2 August where NWP appears to no longer be a good piece of information to utilize. On 2 August, the day started out partly

Table 9. Percentage an Input was Used in the 5 Most Accurate Combinations of all 24 Times

Inputs	10 May	11 May	15 June	2 August	3 August	Overall
Pressure	25	52	53.33	53.33	56.67	49.17
Air Temperature	65	32	50	60	43.33	48.33
Dew Point	65	32	53.33	46.67	43.33	47.5
Measured Particles	75	20	80	66.67	60	60
NWP & MET Obs	65	84	60	40	60	63.33
NWP	10	16	10	6.67	13.33	11.67
Note: Statistics reflect usage of just the individual input mentioned and not ExPERT or climatological GADS information usage						

cloudy and the relative humidity was high for two of the times that were examined on that day. Clouds and increased moisture in the air are conditions that increase the sky radiance compared to a completely sunny day with lower humidity. The conditions on 2 August show how in a saturated atmosphere the measured aerosols, dew point, and air temperature are used more for accurate radiance simulations.

4.2.3 Modeling Issues.

In the process of investigating LEEDR radiance models, a couple issues arose that prevented modeling of radiances for certain days and times. The main issues have to do with atmospheric data that is unavailable for certain times, atmospheric conditions preventing data from being collected, and other factors that skew the data that is collected. All of these things are problems that had to be dealt with or corrected for in order to get the data that would provide a basis for accurate evaluation.

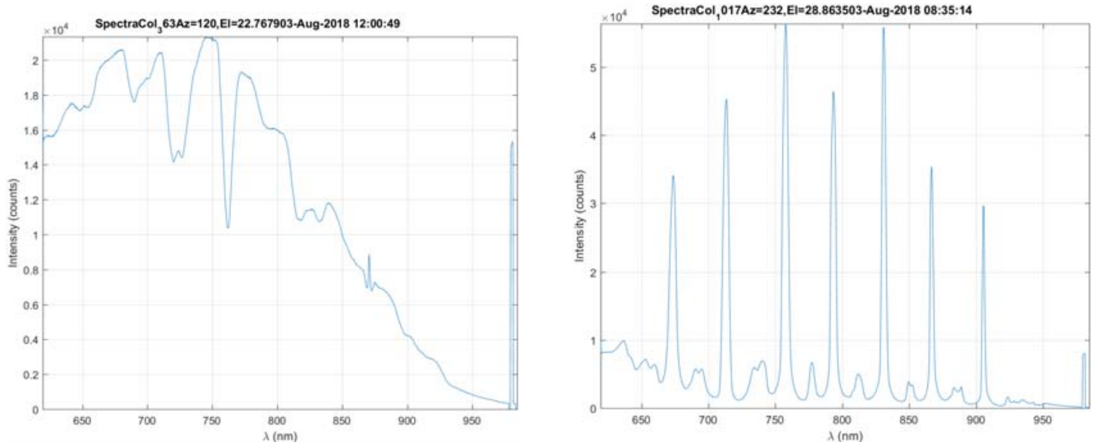

(a) Spectrometer plot of a clear day

(b) Spectrometer plot of a cloudy day

Figure 19. The plots show how spectrometer data looks on clear sunny days compared to data taken on cloudy days.

During the process of selecting days and time to examine, it was necessary to figure out if any of the spectrometer data was taken under nonideal conditions. The presence of clouds drastically changes the intensities over the wavelength range the spectrometer is reading when compared to a clear day as seen in Figure 19. Figure 19a shows the curve produced from spectrometer readings on a clear day are smooth and don't spike anywhere. The spectrometer readings seen in Figure 19b show several spikes at what seems like equidistant wavelengths apart. A cloudy day drastically changes how a radiance plot will look compared to what it looks like on a sunny and clear day where there is nothing in the path of the light going to the spectrometer.

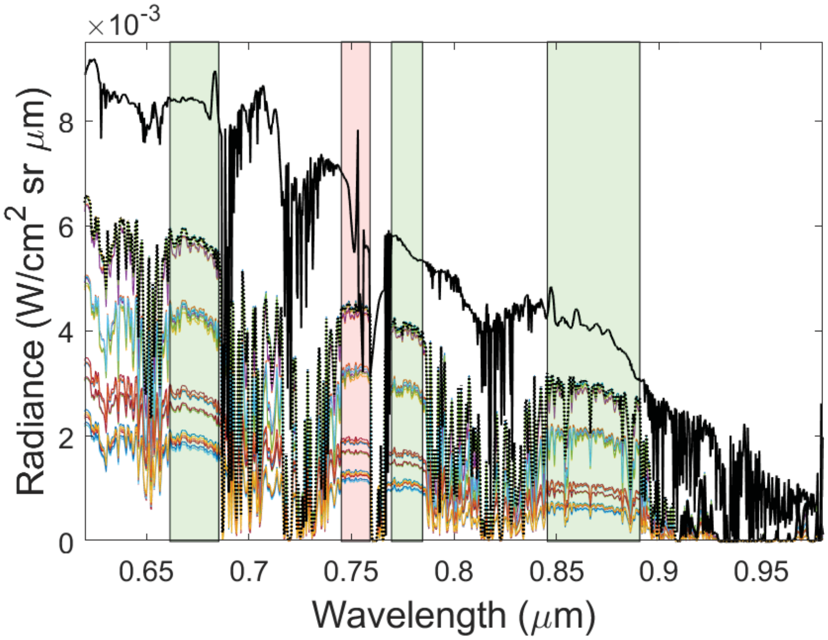

Figure 20. The only instance of the 24 times where the measured radiances were significantly higher than all of the LEEDR radiances.

Another issue that came about in the process of this research are unknown variables that reduce or enhance the amount of sky radiance that is measured. In the process of looking over the comparisons, one of the 24 cases produced significantly higher measured radiances than all of the LEEDR radiance simulations. The case can be seen in Figure 20 and no other days and times showed the measured radiances above all of the LEEDR radiances as is seen in this case.

It is speculated that the increased radiance values for this one day is due to something that got into the path of the spectrometer readings. The spectrometer detects increases in the radiant intensity over the range of wavelengths its measuring across. In this case, it's possible that it was a nearly sunny day and one small cloud moved into the path of where the spectrometer was taking readings in the sky. It is also possible that with a flight line close by a plane flew into the same path that the spectrometer was taking measurements.

(a) The moon rising in the Earth's shadow on 13 November 2016 in Cedarville, OH. Photo by Nathan Fiorino.

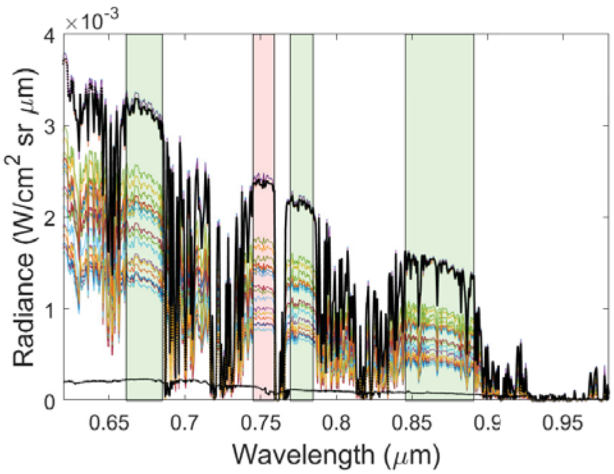

(b) LEEDR and measured radiances at 2030 local time on 10 May 2018

Figure 21. The photo shows how the atmosphere looks when the moon rises in the Earth's shadow and the plot reflects how low sky radiance values are when a spectrometer measures sky radiance in the part of the sky seen in the photo.

Another issue discovered while analyzing the data was at 2030 on 10 May seen in Figure 21. Figure 21a shows the measured radiances are extremely lower than the LEEDR simulated radiances. At this point in time, the Sun is near the horizon while spectrometer readings are taken in the opposite direction of azimuth 148°. The explanation can be seen in Figure 21b where the Moon is seen in a darker level of the sky compared to a slightly brighter level right above it. The two levels are caused by the Sun falling below the horizon so that the Earth's shadow is cast on a lower level of the sky while the Sun's light is cast on the upper level of the sky. The back scattering of the Earth's shadow causes the spectrometer to read a much lower radiance in the sky than is actually there.

V. Conclusions and Future Work

5.1 Overview

This chapter summarizes the research and presents recommendations relative to the original problem and research objectives. It conveys the final conclusions drawn from the results that were found from correlating the radiance characterizations of LEEDR with actual radiance measurements. The chapter also recaps issues that should be followed up on and further research that should be explored in order to determine further effectiveness. Finally, the chapter will ultimately recommend which atmospheric and weather information is needed for LEEDR to come close to duplicating actual sky radiance measurements.

5.2 Conclusions

LEEDR is a very effective radiative transfer code that can calculate the complicated radiative transfer equations and in turn simulate the many atmospheric processes that occur. With the necessary atmospheric information, LEEDR is able to show accurately the transmission, absorption, radiance, and other atmospheric processes. This research was focused on LEEDRs ability to produce accurate radiance characterizations for cloudless conditions given the necessary atmospheric information. The overall problem being addressed in this research is exactly what combination of observed MET data, aerosol particle concentrations, and NWP is necessary to duplicate or come close to real-time measured radiances.

In order to investigate the problem, a comparison needed to be made between real-time radiance measurements and radiance characterizations produced by LEEDR. The comparisons were first used to determine how accurate LEEDR is in characterizing radiances while just relying on surface MET observations and climatological GADS aerosols. After that, comparisons were made in order to determine how close LEEDR can get when using NWP data from GFS or scaled GADS aerosols on their own. Finally, the accuracy of LEEDR radiance characterization was assessed using combinations of MET observations, climatological and scaled GADS aerosols, and NWP data. In addition to that, it was necessary to determine the least amount of information necessary to get the most accurate radiance results.

Initially, Table 5 made it clear that the four input combination groups from Table 4 generally simulate radiances at the same hierarchical levels. The surface MET observations with ExPERT and climatological GADS information typically simulate the highest radiances. The measured aerosol information with ExPERT information and MET observations typically simulate the second highest radiances. The NWP data with climatological GADS information and MET observations typically simulate the third highest radiances. Finally, the NWP data and measured aerosol information with MET observations typically simulates the lowest radiances.

Next, while comparing simulated radiances to measured values, the measurements matched the bottom two hierarchical radiance levels more closely for the majority of the days and times. This observation led to the conclusion that having NWP data greatly aids in accurate radiance characterizations from LEEDR. It also shows LEEDR is least accurate when using MET observations with ExPERT and climatological GADS information. By revealing the inaccuracy in using surface MET observations and climatological GADS information, the first objective has been resolved.

Furthermore, while examining the differences between simulated radiances and measured values, insight is provided relative to those atmospheric inputs that improve the accuracy of LEEDR simulations. First, while looking at the most accurate input combinations in Table 6, it is clear that relying solely on measured aerosol information does not assist with accuracy. Second, simulations based on NWP data are more accurate than simulations based on measured aerosols information. However, NWP data still needs some other piece of atmospheric information in order for LEEDR simulations to come close to measured values. Since measured aerosol information alone and NWP data alone don't quite provide the needed information for accurate simulations, the second objective has also been resolved.

Finally, Table 10 presents the final conclusion which resolves the third objective of the research. From Table 6, it's very evident that measured aerosol information with NWP data and MET observations is required for the most accurate radiance simulations. Beyond that, the next combinations that prove to be most accurate for ra-

Table 10. Top 5 Input Combinations for Accurate Sky Radiances

1. Measured Particles & NWP & MET Observations
2. Measured Particles & NWP
3. NWP & MET Observations & Climatological GADS Information
4. NWP & Climatological GADS Information
5. Measured Particles & MET Observations & ExPERT Information

diance calculations include measured aerosol information with NWP data, NWP data with climatological GADS information and MET observations, NWP data with climatological GADS information, and finally measured aerosol information with MET observations and ExPERT information.

The accuracy of NWP data and measured aerosol information is further confirmed when individual input statistics are explored. Whether you are looking at the 5, 10, or 15 most accurate input combinations over all 24 days and times, the NWP data and measure aerosol information are used the most. Even though they are not used as much, the pressure, air temperature, and dew point are used quite a bit in the most accurate combinations. Also, no MET observation is used more than the others which means they are all equally important in increasing accuracy of simulations.

5.3 Future Work

From here, more work should be done to further investigate how accurate LEEDR can be in reproducing real-time radiance measurements. A few specific areas of research that should be analyzed deal with the wavelength range, the atmospheric information used, the weather conditions, and the aerosol concentrations. The work accomplished here was conducted to specifically examine radiances starting in a small part of the visible band ($0.62\mu m$) and into the NIR ($1\mu m$). By expanding the wavelength range from the UV to the far-IR, a more complete picture of the EM spectrum can be used to test the accuracy of LEEDR radiance simulations. Another area that would provide useful information is introducing less than ideal weather conditions other than clear and sunny summer days. LEEDR can simulate varying weather conditions and knowing the accuracy of LEEDR in those conditions would be greatly beneficial.

The next area that should be looked at is further analysis into the atmospheric information LEEDR uses to get its radiance simulations. First, it would be highly advantageous to determine alternate ways of obtaining the atmospheric information needed for radiance calculations. One such alternate method would be to determine if utilizing aerosol optical thickness measurements from sunphotometers in place of aerosol concentrations is feasible. Second, the top three accurate input combinations in Table 6 include pressure alone, pressure & air temperature, and pressure & dew point respectively. The use of pressure in all of the most accurate cases is an unexpected development since the expectation was the air temperature and dew point play a greater role in accurate radiance calculations. It would be beneficial to further study why pressure was more important in the most accurate input combinations.

5.4 Summary

Ultimately, no single atmospheric LEEDR input was found to improve LEEDR radiance characterizations so they duplicate real-time measured sky radiances. NWP data and measured aerosol information appears to be the most important inputs for accurate simulations. In addition, not one MET observation is more important than the other for accuracy but including one or more with NWP data and measured aerosol information has been shown to increase accuracy. In the future, further investigations should dwell on a number of different areas that could assist in advancing this research further. The areas include utilizing a broader range of wavelengths, introducing less than ideal weather conditions, further determining the importance of the three MET observations, and finding alternate atmospheric information that can be used in simulations.

Bibliography

1. G. Aiyan, C. Jingshuang, Z. Aosong, and H. Shanbao. Attenuation and Sky Radiance Effects Induced by Atmospheric Aerosols on Satellite-Ground Optical Communications Links. In *9th IEEE International Conference on Communication Software and Networks*, pages 619–623, May 2017.

2. Atomic and Molecular Physics Division, Harvard-Smithsonian Center for Astrophysics. HITRAN Online. URL `https://hitran.org/`, 2018.

3. A. Berk, P. Conforti, R. Kennett, T. Perkins, F. Hawes, and J. van den Bosch. MODTRAN6: A major upgrade of the MODTRAN radiative transfer code. In *Algorithms and Technologies for Multispectral, Hyperspectral, and Ultraspectral Imagery XX*, volume 9088, June 2014.

4. R. Boyd. *Radiometry and the Detection of Optical Radiation*. John Wiley & Sons, Inc., 1st edition, 1983.

5. K. Bullrich. Scattered Radiation in the Atmosphere and the Natural Aerosol. In *Advances in Geophysics*, volume 10, pages 99–260. Elsevier, January 1964.

6. J. Burley, S. Fiorino, B. Elmore, and J. Schmidt. A Fast Two-Stream-Like Multiple-Scattering Method for Atmospheric Characterization and Radiative Transfer. In *Journal of Applied Meteorology and Climatology*, volume 56, pages 3049–3063, November 2017.

7. Center for Directed Energy. *LEEDR User Guide*. Air Force Institute of Technology, Version 4.0, 2018.

8. Davis Instruments Corp. *Console for Vantage Pro2 and Vantage Pro2 Plus Weather Stations*. Davis Instruments Corp., Revision M, 2015.

9. H. Evans, J. Lange, and J. Schmitz. *Phenomenology of Intelligence-focused Remote Sensing*, volume 1: Electro-optical Remote Sensing. Riverside Research, 2015.

10. S. Fiorino, R. Bartell, M. Krizo, K. Moore, and S. Cusumano. Validation of a Worldwide Physics-based, High Spectral Resolution Atmospheric Characterization and Propagation Package for UV to RF Wavelengths. In *Proceedings of SPIE - Atmospheric Optics: Models, Methods, and Target-in-the-Loop Propagation II*, volume 7090, August 2008.

11. S. Fiorino, R. Bartell, M. Krizo, K. Moore, and S. Cusumano. A First Principles Atmospheric Propagation and Characterization Tool - The Laser Environmental Effects Definition and Reference (LEEDR). In *Proceedings of SPIE - Atmospheric Propagation of Electromagnetic Waves II*, volume 6878, January 2015.

12. S. Fiorino, K. Keefer, C. Rice, J. Burley, and J. Schmidt. Characterizing Multispectral Vertical Profiles of Aerosol Extinction with Surface-based Measurements. In *Imaging and Applied Optics*, June 2017.

13. S. Fiorino, S. Peckham, J. Schmidt, and K. Keefer. Evaluation of Aerosol Characterizations within the WRF-Chem GOCART Scheme. Submitted to the Journal of Applied Meteorology and Climatology, 2019.

14. S. Fiorino, R. Randall, M. Via, and J. Burley. Validation of a UV-to-RF Spectral Resolution Atmospheric Boundary Layer Characterization Tool. In *Journal of Applied Meteorology and Climatology*, volume 53, pages 136–156, January 2014.

15. S. Fiorino, S. Shirey, A. DeMarco, P. He, and S. Basu. Capturing Realistic Boundary Layer Aerosol and Turbulence Effects in WRF and Other Numerical

Weather Models. In *Propagation Through and Characterization of Distributed Volume Turbulence*. Imaging and Applied Optics Conference, June 2015.

16. E. Hecht. *Optics*. Pearson Education, Inc., 5th edition, 2017.

17. M. Hess, P. Koepke, and I. Schult. Optical Properties of Aerosols and Clouds: The Software Package OPAC. In *Bulletin of the American Meteorological Society*, volume 79, pages 831–844, May 1998.

18. Kanomax USA, Inc. *Kanomax Handheld CPC Model 3800*. Kanomax USA, Inc., 2014.

19. P. Koepke, M. Hess, I. Schult, and E. Shettle. Global Aerosol Data Set. Max-Planck-Institut fur Meteorologie, September 1997.

20. C. Levoni, M. Cervino, R. Guzzi, and F. Torricella. Atmospheric Aerosol Optical Properties: A Database of Radiative Characteristics for Different Components and Classes. In *Applied Optics*, volume 36, pages 8031–8041, October 1997.

21. Meade Instruments Corporation. *8", 10", 12", 14", 16" LX200-ACF Advanced Come-Free Telescopes with GPS and AutoStar II Hand Controller*. Meade Instruments Corporation, 2009.

22. National Oceanic and Atmospheric Administration. NCEI Global Forecast System (GFS). URL `https://www.ncdc.noaa.gov/data-access/model-data/model-datasets/global-forcast-system-gfs`, 2018.

23. National Oceanic and Atmospheric Administration. NCEI Weather Model Data. URL `https://www.ncdc.noaa.gov/data-access/model-data`, 2018.

24. Ocean Optics Inc. *QE65000 Scientific-grade Spectrometer Installation and Operation Manual*. Ocean Optics Inc., 2007.

25. G. Petty. *A First Courses in Atmospheric Radiation*. Sundog Publishing, 2nd edition, 2006.

26. G. Thomas and R. Cobb. Daytime Sky Brightness Characterization for Persistent GEO SSA. In *Advanced Maui Optical and Space Surveillance Technologies Conference*, September 2017.

27. TSI Incorporated. *Nano Water-based Condensation Particle Counter*. TSI Incorporated, Revision C, 2013.

REPORT DOCUMENTATION PAGE

Form Approved
OMB No. 0704–0188

1. REPORT DATE *(DD–MM–YYYY)*	2. REPORT TYPE	3. DATES COVERED *(From — To)*
21–03–2019	Master's Thesis	Sep 2017 – Mar 2019

4. TITLE AND SUBTITLE

Coupled Atmospheric Surface Observations with Surface Aerosol Particle Counts for Daytime Sky Radiance Quantification

5a. CONTRACT NUMBER

5b. GRANT NUMBER

5c. PROGRAM ELEMENT NUMBER

6. AUTHOR(S)

Wolfmeyer, Scott S, 1Lt, USAF

5d. PROJECT NUMBER

19P-313; 19P-319

5e. TASK NUMBER

5f. WORK UNIT NUMBER

7. PERFORMING ORGANIZATION NAME(S) AND ADDRESS(ES)

Air Force Institute of Technology
Graduate School of Engineering and Management (AFIT/EN)
2950 Hobson Way
Wright Patterson AFB, OH 45433-7765

8. PERFORMING ORGANIZATION REPORT NUMBER

AFIT-ENP-MS-19-M-095

9. SPONSORING / MONITORING AGENCY NAME(S) AND ADDRESS(ES)

Directed Energy - Joint Transition Office
801 University Blvd. SE, Suite 100
Albuquerque, NM 87106

10. SPONSOR/MONITOR'S ACRONYM(S)

DE-JTO

11. SPONSOR/MONITOR'S REPORT NUMBER(S)

12. DISTRIBUTION / AVAILABILITY STATEMENT

Distribution Statement A.
Approved for Public Release; Distribution Unlimited.

13. SUPPLEMENTARY NOTES

14. ABSTRACT

This study investigates the radiative transfer code, Laser Environmental Effects Definition and Reference (LEEDR), developed by the Center for Directed Energy at the Air Force Institute of Technology. Many multi- and hyperspectral applications are limited to the nighttime due in large part to daytime solar background noise and it is advantageous to be able to quantify this background noise using LEEDR. Real-time meteorological surface observations, numerical weather prediction, and aerosol particle concentrations were used to investigate the accuracy of LEEDR radiances simulations. Comparisons between simulations and measured values show that aerosol concentrations, weather predictions, and meteorological observations provide enough information to nearly duplicate real-time measured sky radiances.

15. SUBJECT TERMS

Laser Environmental Effects Definition and Reference (LEEDR), meteorological surface observations, numerical weather prediction, aerosol particle concentrations

16. SECURITY CLASSIFICATION OF:			17. LIMITATION OF ABSTRACT	18. NUMBER OF PAGES	19a. NAME OF RESPONSIBLE PERSON
a. REPORT	b. ABSTRACT	c. THIS PAGE			Dr. Steven Fiorino, AFIT/ENP
					19b. TELEPHONE NUMBER *(include area code)*
U	U	U	UU	77	(937)255-3636 x4506; steven.fiorino@afit.edu

Standard Form 298 (Rev. 8–98)
Prescribed by ANSI Std. Z39.18